Synthesis and Evaluation of Radiopharmaceuticals for Imaging Bacterial Infection

Synthesis and Evaluation of Radiopharmaceuticals for Imaging Bacterial Infection

By

Omid Beiraghi

B.Sc. (University of Windsor) B.A. (University of Windsor) 2013

A Thesis

Submitted to the School of Graduate Studies

In Partial Fulfillment of the Requirements

For the Degree of

Masters of Science

Chemistry

McMaster University

Masters of Science (2015) McMaster University

(Chemistry) Hamilton, Ontario

TITLE: Synthesis and Evaluation of Radiopharmaceuticals for Imaging Bacterial Infections

Author: Omid Beiraghi, B.Sc. (University of Windsor), B.A. (University of Windsor)

Supervisor: Dr. John F. Valliant

Number of Pages: 98

Abstract

Despite recent advances, radiopharmaceuticals to detect and characterize bacterial infections have a number of limitations. Many of the clinically approved radiopharmaceutical agents are not specific to bacterial infections and accumulate at lesions of inflammation. Hence, new approaches are necessary to detect bacteria with high specificity and selectivity. A library of desferrioxamine B (DFO) derivatives were prepared to create radiolabeled siderophores to create a bacteria-specific imaging probe by exploiting the mechanism bacteria use to scavenge iron, which plays a key role in bacterial growth and biofilm formation Compounds were synthesized using two convenient carbamate forming strategies in 30% to 92% yield. The cold and radioactive gallium (^{67}Ga) complexes were prepared and characterized and their uptake by *S. aureus* bacteria were assessed *in vitro* and *in vivo*. *In vivo* studies revealed that ^{67}GaDFOethoxycarbamate had uptake comparable to GaDFO that was blockable, showing the compound was actively taken up via the siderophore pathway. *In vivo* studies in a mouse model resulted in a good infected to non-infected thigh ratio (11:1) and non-specific uptake by the GI tract.

Bioorthogonal chemistry was also explored as an approach for imaging infection using *trans*-cyclooctene (TCO) functionalized vancomycin and a tetrazine functionalized ^{67}GaDFO (^{67}GaDFO-Tz) complex.[2,3] *In vitro* results revealed that allowing vancomycin-TCO to bind *S. aureus* prior to the addition of ^{67}GaDFO-Tz (pretargeting) showed higher

(63%) uptake than with a conjugate formed prior to incubation with the bacteria (direct targeting, 28%). For the bioorthogonal approach, the distribution of the ^{67}GaDFO-Tz was assessed in a *S. aureus* infection murine model, which showed significant uptake of ^{67}GaDFO-Tz in the GI tract 1 h post intravenous injection. However, uptake in the infected joint was evident at 71 h post infection. The data suggests targeting bacteria using TCO-labeled antibiotics and radiolabeled tetrazines is a feasible strategy, but that further optimization of the vancomycin injection dose and injection time are necessary.

Acknowledgements

I would like to express my sincerest gratitude to an incredible group of people, without whom this thesis would have not been possible. Firstly, I would like to express my sincerest gratitude to my supervisor, Prof. John Valliant, for his mentoring and support throughout the past two years. He has challenged and inspired me to reach my potential, and for that I am truly grateful. I would like to thank my committee members, Prof. John Brennan and Prof. Paul Berti, for their guidance throughout my project and for taking their time to read my thesis. I would like to thank Dr. Kirk Green for his help and support with Mass Spec, and his humour which has brightened my day on many occasions.

I would also like to thank all of my amazing friends and colleagues in the past and present that have been a part my life. I would like to extend my thank you to all of the members of the Valliant group and all of the amazing people that I have met at McMaster. I would like to express my deepest gratitude to Dr. Joseph Ioppolo for all of his help, encouragement, and support during my first few months at McMaster. He has been an incredible mentor, colleague, and a friend. I would like to thank Patricia Edem for being a truly amazing friend, volunteer buddy, and a great neighbour from day 365. I would like to thank Reza Yazdani for all of his pep talks and wise words, and for his jokes and humour to cheer me up. I would also like to thank Reza for feeding me sweets and tea! I would like to thank Salma Al-Karmi for her entertaining personality. I would

like to thank Ignace Moya for his exceptional character and his incredibly wild stories. I would like to thank Stephanie Rathmann for her sunny personality. I would like to thank for her positive and upbeat character. I would like to thank Sheilan Sinjari for her upbeat personality that has brightened my day on so many occasions. I would like to thank Negin Balaghi for being an incredible friend since my first week in Hamilton. I would like to thank Roxana Barbu for being an amazing sister and listening to my rants from 516 Km away. I would like to thank Dan Duong for all of our scientific and at times the most random discussions, and of course for being truly an exceptional friend. I would like to thank Qinyuan Zhou for her jokes, humour and support to cheer me up when I'm feeling down and to throw me back down when I'm too happy.

I would also like to extend my deepest gratitude to Prof. Holger Eichhorn and Prof. James Gauld for all their mentoring and support during my undergraduate years and beyond.

I would like to thank my family for all of their love and support. I am grateful for my mother, Mina Shiva, for her unconditional love and support. I am grateful for my father, Houshang Beiraghi, for always encouraging me to achieve my dreams.

Table of Contents

Table of Figures

Table of Schemes

Tables

List of Abbreviations

BAI	Biomaterial associated infection
Bq	Becquerel
CFU	Colony Forming Units
CT	Computed Tomography
CV	Crystal Violet
d	Doublet
DFO	Desferrioxamine B
EC	Electron Capture
FDA	Food and Drug Administration (Unites States of America)
FDG	Fluorodeoxyglucose
FDS	Fluorodeoxysorbitol
FOXE	Ferrioxamine E
FSC	Fusarinine C
FUO	Fever of Unknown Origin
h	hour(s)
HPLC	High Performance Liquid Chromatography
Hz	Hertz

ID	Injected Dose
IR	Infrared Spectroscopy
LT	Left Thigh
m	Multiplet
MBq	MegaBecquerel
MDP	maltodextrin-based imaging probes
MFNP	Magnetically Fluorescent Nanoparticles
min	Minutes
mp	Melting Point
MRI	Magnetic Resonance Imaging
MS	Mass Spectrometry
NIRF	Near-Infrared Fluorescence
NMR	Nuclear Magnetic Resonance
PBS	Phosphate-buffered saline
PET	Positron Emission Tomography
p.i.	Post injection
PK	pharmacokinetics
ppm	Parts per million
R_f	Retention Factor
RGD	Arginylglycylaspartic acid
RT	Right Thigh
s	Singlet

SEM	Standard Error Mean
SPECT	Single Photon Emission Computed Tomography
t	Triplet
TAFC	triacetylfusarinine C
TCO	*Trans*-cyclooctene
TFLI	Targeted Fluorescent Imaging
Tz	Tetrazine
US	Ultrasound
UV	Ultraviolet
µNMR	Micro Nuclear Magnetic Resonance

Chapter 1

1 Introduction

1.1 Bacterial Infections

Bacterial infections are a common cause of mortality, especially amongst cancer and post-surgical patients.[1] Hence, early diagnosis and localization of hidden bacterial infections are crucial and remain a critical healthcare challenge globally. Infection is defined as the invasion and multiplication of pathogens which may result in tissue damage from various cellular or toxic processes.[2] Progression of infections can eventually lead to tissue damage and even death to the host if not controlled.[2] With respect to infections acquired during hospitalization, about 60% are caused from ESKAPE bacteria; these are *Enterococcus faecium*, *Staphylococcus aureus*, *Klebsiella pneumoniae*, *Acinetobacter baumannii*, *Pseudomonas aeruginosa*, and *Enterobacter* species.[3]

The development of better diagnostic techniques for detecting bacteria is the key to improving treatment and requires an understanding of the basic biology of bacteria and their impact on human health. With respect to the former, the cell walls of bacteria are composed of the crosslinked polysaccharides, peptidoglycans.[4] Bacteria are classified into Gram-positive and Gram–negative based on the properties of the cell wall determined by Gram staining.[5] The gram staining process involves treating bacteria with

a crystal violet-iodine complex and safranin counterstain followed by subsequent treatment with alcohol. Gram positive bacteria have several layers of peptidoglycans and thick cell walls while Gram-negative bacteria have few layers of peptidoglycans (less than Gram-positive bacteria) and hence, thinner cell walls.[4] Furthermore, while Gram-positive bacteria consist of a thick peptidoglycan layer and capsule on its outer membrane, Gram-negative bacteria consist of peptidoglycan by its periplasmic space and phospholipid bilayer, lipopolysaccharide, and capsule on its outer membrane.[4] Gram-positive bacteria retain the dye complex and remain purple while the Gram-negative bacteria decolour.[5]

Bacteria exist in both planktonic and biofilm states. Planktonic bacteria are free floating, while biofilms are comprised of a larger group of bacteria that have adhered to a surface and are encased in an extracellular polymeric membrane.[6] This polymeric membrane protects the bacteria in a hostile environment where they become less susceptible to conventional antibiotic treatments.[6] As a result, biofilms are difficult to diagnose and treat in patients. As an example, *S. epidermidis* and *S. aureus* are common hospital-acquired biofilm bacterial species prominent in orthopedic device implants.[6] Currently, these types of biofilms are diagnosed through blood tests or indirect techniques such as X-ray, ultrasound, or magnetic resonance imaging, which are often inconclusive.

A related and major clinical issue is fever of unknown origin (FUO). It is defined by an elevated body temperature greater than 38.3 °C that persists more than 3 weeks without a diagnosis, despite one week of inpatient investigation. One study at Kitasato

University Hospital in Japan showed that FUO accounts for 3% emergency room admissions and it may be due to a variety of different conditions such as cancer, autoimmune diseases, inflammatory disorders, or bacterial infections; the most common (one-third) being the latter.[7,8] FUO diagnosis involves physical examination, blood tests, and radiographic studies, which often lead to false negative results.[8] As a result, FUO is typically treated with broad spectrum antibiotics which may not be necessary, thus promoting bacterial resistance. Bacterial resistance is emerging as a serious global health care issue that is caused by overuse of antibiotics.[3] Attempts to combat overuse are actively being pursued to minimize the further development of antibiotic resistant bacteria.[8] Beyond unnecessary treatment, prolonged diagnosis times can further deteriorate the health of patient's with FUO.

Infections in the elderly are of particular importance due to age related changes in their immune function.[9,10] Seniors with immunosenescence, gradual age related deterioration of an individual's immune function, are more prone to acute infections and autoimmune diseases.[9] In many cases, treatment of infections will result in the development of late onset autoimmune and other inflammatory diseases. Hence, it is important to accurately discriminate infections from inflammation. Furthermore, better diagnostic tools are necessary to monitor the progress of treatment.

Biomaterials associated infections (BAI) are also becoming a challenge in healthcare due to the aging population and increased use of medical implants.[11] Typically, BAIs on implants result from bacterial biofilms, which adhere to the surface of the implanted material where they are less susceptible to the host defense system.[12,13] As

a result, their treatment through conventional techniques becomes a challenge. Coagulase-negative *staphylococci* and *S. aureus* are the most common cause of BAI hospital-acquired pathogenic infections where they account for two-thirds of prosthetic joint infections in North America.[14,15] Driven by FUO and BAI, and that fact that bacterial infections are among the leading causes of mortality worldwide, there is an active search for better diagnostic tools for imaging infection.[16]

1.2 Current Techniques for Diagnosing Infections and their Limitations

Detection of bacterial infections at an early stage is important for treatments to be effective.[17] Current techniques such as X-ray, ultrasound (US), computed tomography (CT), and magnetic resonance imaging (MRI) are only useful at later stages of infection once it has caused significant tissue damage. Furthermore, these techniques are not specific for visualizing infections but rather actually show the resulting tissue damage that has occurred due to the infection. Biomarker and blood tests are also not ideal as they are generally only effective once infections have spread sufficiently. Nuclear medicine based imaging techniques such as single photon emission computed tomography (SPECT) and positron emission tomography (PET) have been used in an attempt to address some of these issues.

1.3 Nuclear Molecular Imaging

Nuclear medicine imaging involves the administration of radiopharmaceuticals that allow the visualization, assessment, and measurement of physical, cellular, and

biochemical process *in vivo*.[18] Nuclear techniques have the potential to visualize infections, directly, at early stages. The two main nuclear medicine imaging techniques are SPECT and PET. PET and SPECT have high sensitivity, in that radiopharmaceuticals can be detected using very small quantities of probe, and specificity, which refers to the differentiation of positive signals from negative ones.[17,19] Hybrid imaging systems such as PET-CT and SPECT-CT, which are now available in nearly all hospitals, generate both functional and anatomical information from the same study.[19]

1.4 Positron Emission Tomography

Radionuclides used for PET are positron emitting. Positrons travel a short distance through matter where they combine with an electron and undergo an annihilation process to emit two gamma ray photons of 511 keV. These collinear gamma rays are detected in coincidence by a ring of detectors that surround the patient.[19] Images are reconstructed to give rise to 3-D or 4-D (time) datasets. PET agents that have been used for imaging infection have been derived from a variety of different isotopes including ^{68}Ga, ^{18}F, and ^{89}Zr. Examples include ^{18}F-labeled maltohexaose, ^{18}F-labeled fluorodeoxysorbitol, and ^{68}Ga-citrate which are further described below.[20–22]

1.4.1 Single Photon Emission Tomography

In contrast to PET, SPECT radionuclides generally emit lower energy gamma rays which are detected by gamma cameras.[19] The gamma camera is rotated around the patient in small increments to acquire 2-D images from various angles. Subsequently,

tomographic reconstruction is applied to give rise to a 3-D dataset. Transverse, sagittal, and coronal images can be produced from the dataset.[19] The most commonly used SPECT isotopes are ^{67}Ga, ^{99m}Tc, ^{111}In and ^{123}I. Gallium-67 ($t_{1/2}$=78.2 h), which was used in this thesis, decays by electron capture (EC) which results in the production of γ-rays with energies of 93 keV, 184 keV, 300 keV, and 393 keV.[18]

1.4.2 Current Nuclear Medicine Techniques for Detecting Bacterial Infection

Current nuclear medicine bacterial imaging agents used in clinics include ^{18}F-fluorodeoxyglucose (^{18}F-FDG), ^{67}Ga-citrate, and ^{111}In- or ^{99m}Tc-labeled leukocytes.[23–25] The problem with these radiopharmaceuticals is that they are either not specific to bacterial infections, failing to discriminate bacterial infections from inflammation, or they have low uptake by bacteria or, in the case of ^{67}Ga-citrate, the agent exhibits slow clearance from non-target tissues and therefore require long imaging times. There is a need to develop radiopharmaceuticals that can selectively target bacterial infections *in vivo*. Ideal imaging agents must localize rapidly at the site of infection and clear from non-infected tissues. Moreover, they must be able to discriminate infection from inflammation. One approach to creating such compounds is to develop tracers that target biochemical pathways specific to bacteria.

1.5 Emerging Imaging Techniques for Detecting Bacterial Infection

1.5.1 Targeted Fluorescent Imaging

Optical imaging, more specifically targeted fluorescent imaging (TFLI), is an emerging imaging technique that allows for direct, non-invasive, and high resolution

imaging of bacteria in humans.[11,26] It has also been used for intraoperative bacteria-specific fluorescence imaging. For example, Oosten *et al.* used fluorescently labeled vancomycin (vancomycin-IRDye 800CW) to specifically target and detect Gram-positive bacteria using optical imaging.[11] They demonstrated the specificity and selectivity of the imaging agent towards Gram-positive bacteria and its ability to discriminate infection from sterile inflammation using murine and human post-mortem models.

Ning *et al.* used a maltodextrin-based fluorescent imaging probe (MDP) to detect metabolically active bacteria *in vivo*.[27] Maltohexaose is a source of glucose for bacteria and is internalized by the bacteria-specific transporter; therefore, MDPs were used to target the maltodextrin transport pathway in metabolically active bacteria. Their results demonstrated that MDPs can discriminate sterile inflammation from active bacteria with a limit of detection of 10^5 colony forming units (CFUs).

A major challenge for the clinical implementation of optical techniques results from attenuation of the signal even with near-infrared fluorescence (NIRF) probes, which have a maximum tissue penetration of 1 cm.[11] Therefore, deeply seated infections cannot be detected non-invasively.[11,28] Nevertheless, using the appropriate probe, these experiments show that it is possible to selectively image specific biomaterials associated Gram-positive bacteria *in vivo*.

1.5.2 Magnetic Detection

Magnetic based methods represent an emerging class of techniques to detect infections. Magnetic detection is sensitive, rapid, and relatively inexpensive.[4,29] Magnetic detection devices include miniaturized micro nuclear magnetic resonance (μNMR)

devices, magnetoresistance devices, and Hall effect sensors. For example, Budin *et al.* used a magnetic Gram stain approach to tag bacterial infections *in vitro*.[4] Crystal violet-*trans*-cyclooctene (CV-TCO) was used to label bacteria, which was followed by treatment with magnetofluorescent nanoparticles (MFNPs) that reacted with the TCO groups to allow for the imaging of bacteria as a multimodal optical and magnetic imaging agents. Having shown that TCO tagged bacteria can be prepared, there is the opportunity to build on this chemistry to develop new *in vivo* MRI probes for bacteria.

Trans-cyclooctene (TCO) derivatives of vancomycin and daptomycin in place of Gram stains have also been used as targeting vectors that were subsequently labeled using MFNP.[30] Chung *et al.* demonstrated the detection of Gram-positive bacteria with MFNPs using a similar approach which showed two-fold greater sensitivity than with direct targeting (i.e., linking vancomycin-TCO or daptomycin-TCO to MFNP-tetrazine prior to incubation with bacteria).[30] Furthermore, their results showed vancomycin to have more effective binding to Gram-positive bacteria than daptomycin, despite their similar binding mechanism.

1.6 Novel PET and SPECT Agents

The promising results of maltodextrin-based fluorescent imaging probe described above led to the development of ^{18}F-labeled maltohexaose by Ning *et al.* to image metabolically active bacteria *in vivo* with high sensitivity and specificity.[12] More recently, ^{18}F-labeled fluorodeoxysorbitol (^{18}F-FDS) was developed by Weinstein *et al.* to successfully image Enterobacteriaceae infections *in vivo*.[13] Sorbitol is a substrate that is specifically metabolized by Enterobacteriaceae and hence, it does not accumulate in

Gram-positive bacteria, aerobic Gram-negative rod, or mammalian and tumour cells. These developments notwithstanding, there remains a need to develop molecular imaging probes to selectively detect bacterial infections *in vivo*. The ideal imaging agent would rapidly localize at the site of infection correlating with the type and extent of infection and clear from non-infected tissues. A viable agent should also be able to discriminate bacterial infection from sterile inflammation and be useful for both Gram positive and negative bacteria.

1.7 Radiolabeled Siderophores

Iron is essential for most microorganisms, including bacteria, due to its role in electron transport and metabolic processes.[31] Despite its abundance, $Fe(OH)_3$ is insoluble in aerobic environments; hence, microorganisms have evolved ways to scavenge and take up iron. Siderophores are low molecular weight compounds released by bacteria, fungi, and some plants to scavenge for iron from their environment.[31] Once bound to Fe^{3+}, these siderophores are then actively taken up by bacteria. Siderophores have a high selectivity and affinity (K_a values up to 10^{52} M^{-1}) towards iron.[31] For example, the K_a values for DFO and enterobactin are reported to be greater than 10^{30} M^{-1} and 10^{52} M^{-1}, respectively.[32,39] Ga^{3+} has comparable ionic radius, charge, and electronic configuration to Fe^{3+} and thus, it can be used as an iron mimetic.[33] More specifically, the ionic radii of Ga^{3+} and Fe^{3+} are 62 pm and 64.5, respectively. Fortuitously, there are two medical isotopes of gallium that can be used for SPECT and PET imaging (^{67}Ga and ^{68}Ga).

Radiolabeled siderophores have been reported in the literature for potential applications in imaging infections and fungi.[34–36] Biodistribution, labeling efficacy, protein binding, and stability has been shown to vary between different siderophores.[34] Studies by Petrik *et al.* revealed that triacetylfusarinine C (TAFC) and ferrioxamine E (FOXE) (Figure 1.1) have high affinity towards ^{68}Ga, and when complexed exhibit excellent metabolic stability and high specific uptake in *Aspergillus fumigatus*, a pathogenic fungus associated with lung infections.[34] Moreover, these agents have good biodistribution profiles in mice models with rapid renal and blood clearance, and low non-specific binding in other organs.

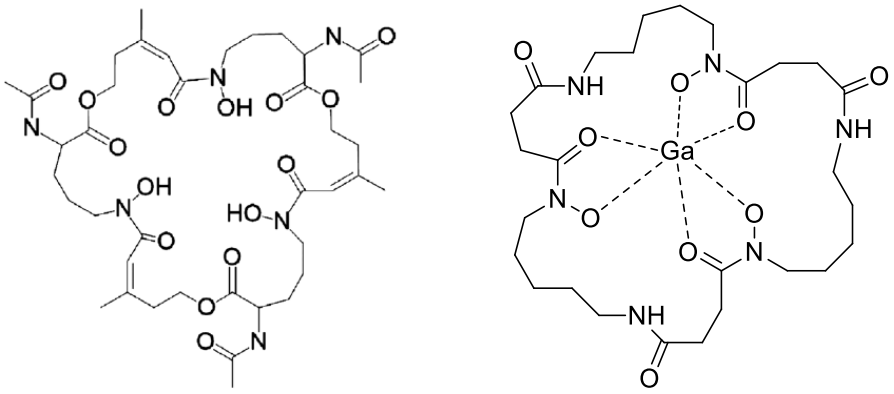

Figure 1.1 Structures of TAFC (left) and GaFOXE (right)

Siderophores are also increasingly being used as bifunctional chelators, which are compounds that have functional groups to chelate a metal and conjugate to a targeting construct. For example, fusarinine C (FSC), a siderophore-based bifunctional chelator, can be labeled with ^{68}Ga resulting in high radiochemical yield over a wide pH range in the presence of other metal (Fe^{3+}, Al^{3+}, Zn^{2+}) impurities.[33] It also has 3 free amines which

can be used to couple the chelate to a targeting vector, hence making this a suitable agent for developing molecular imaging probes.[33] For example FSC derivatized RGD has been reported as a tracer for imaging tumour angiogenesis.[33,37]

1.8 Desferrioxamine B

Desferrioxamine B, referred to as DFO, is a common bacterial siderophore that is commercially available. DFO is one of first siderophore based bifunctional chelators to be radiolabeled with $^{67/68}$Ga.[38] The binding constant of Fe-DFO is reported to be between 10^{30} and 10^{31} M^{-1}, which is expected to be similar for Ga-DFO (Figure 1.2).[39] This can be explained by the comparable ionic radii, coordination chemistry, and electronic confirguration between Fe^{3+} and Ga^{3+}.[33] DFO is FDA approved for iron chelation therapy where the hydroxamates chelate Fe^{3+} to form a hexadentate metal complex. A major challenge of using DFO for imaging infections is its poor pharmacokinetic (PK) properties in that it is rapidly cleared prior to uptake at the site of infection. If DFO is to be used as a way to image bacterial infections, PK modification would be necessary, which is the focus of Chapter 2 of this thesis.

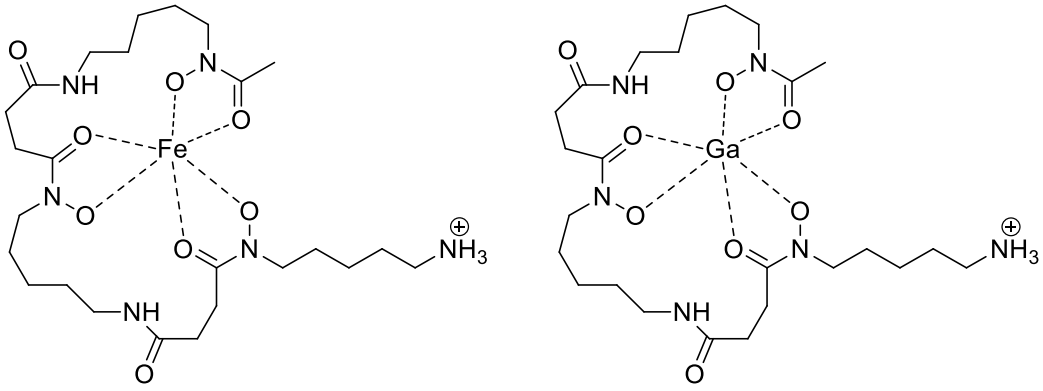

Figure 1.2 Structures of Fe-DFO (left) and Ga-DFO (right)

In addition to its use as imaging tracers, GaDFO can also be used as a therapeutic agent.[40] Due to the similar properties of Ga^{3+} and Fe^{3+} and the inability of Ga^{3+} to undergo redox chemistry *in vivo*, gallium can compete with iron and interfere with bacteria's iron metabolism pathways. As a result, DFO can serve as a means to transport the toxic gallium to bacterial cells. Banin *et al.* have shown GaDFO in conjunction with antibiotics to be more effective at killing planktonic bacteria and preventing biofilm formation *in vitro* and *in vivo* than the antibiotics alone.[40] Because of the aforementioned issue of poor pharmacokinetic properties, the therapeutic utility of GaDFO is limited. As a result, the non-radioactive gallium complexes of any promising radiolabeled DFO derivatives which show improved pharmacokinetics can potentially be used as a way to enhance the efficacy of antibiotics.

1.9 Targeting Bacterial Infections using Antibiotics

1.9.1 Antibiotics

Directly targeting bacteria using radiolabeled antibiotics represents an alternative to siderophore based agents for imaging infections. Antibiotics are the largest class of targeting vectors for bacterial infections and they offer constructs with high affinity and specificity towards bacteria.[17] Several antibiotics have been radiolabeled to study their pharmacokinetics and as infection imaging agents. Ciprofloxacin is the most extensively studied, where ^{99m}Tc-ciprofloxacin was developed commercially as an infection imaging agent.[41–43] However, recent studies have re-examined ^{99m}Tc-cirpofloxacin and revealed this agent to be non-specific towards bacterial infections noting it also accumulates at sites of inflammation.[44–46] Other radiolabeled antibiotic in literature include B-lactam antibiotics such as cephalosphorins,[47–51] aminoglycosides,[52,53] phosphonodipeptides,[54] glycopeptides,[55–57] and others.[58–61]

Many of these antibiotics, like the ciprofloxacin derivatives, are not specific towards bacterial infection and accumulate at sites of inflammation. In contrast, vancomycin has been shown to have potential as bacteria specific imaging agent.[11,30,56,62] As previously noted, vancomycin derivatized with a fluorescent dye has been used to image bacteria through fluorescence imaging. Unfortunately, clinical translation is hindered by the limited sensitivity, depth of penetration and difficulties associated with quantification of fluorescent imaging.[63] Nevertheless, it may be possible to build on this

approach and develop a radiolabeled analogue for use with nuclear medicine based techniques which is the focus of Chapter 3 of this thesis.

1.10 Objectives and Description of Contributions

Despite reports of new techniques such as magnetic detection and targeted fluorescent imaging (TFLI), imaging bacterial infections using nuclear medicine techniques remains an attractive choice because of the potential to achieve high sensitivity and specificity. This thesis describes two approaches to creating the radiopharmaceuticals needed to use nuclear imaging methods to image infection where the first involved the synthesis and radiolabeling of DFO derivatives (Chapter 2). The second strategy explored the use of radiolabeled antibiotics and bioorthogonal chemistry to image bacteria through direct and pretargeted techniques (Chapter 3).

The second chapter of this thesis involves the modification of DFO to enhance its pharmacokinetic properties, which was done in collaboration with a post-doctoral fellow Dr. Joe Ioppolo. For clarity, DFO *n*-hexyl, DFO *N*-quinoline, DFO *n*-hexyl carbamate, and DFO *n*-hexylamine-Boc carbamate, and DFO *n*-hexylamine carbamate derivatives and their respective metal ligands were prepared and characterized by Omid Beiraghi. Furthermore, radiometal complexes of all DFO ligands described in Chapter 2 was prepared by the author. The *in vivo* studies were done by Megan Blacker while the cell uptake studies were performed by Lisset Llano and Deanna Caldwell.

Chapter 3 describes the use of a ^{67}GaDFO tetrazine derivative to label a *trans*-cyclooctene (TCO)-vancomycin derivative directly and via a two-step pretargeting type strategy. As a first step, vancomycin norbornene derivatives were prepared to optimize

the bioorthogonal chemistry prior to working with *trans*-cyclooctene. The norbornene and *trans*-cyclooctene derivatives of vancomycin, DFO ligand and its respective metal and radiometal complexes were prepared by the author. The *in vivo* studies were done by Megan Blacker. The cell uptake studies were done by Lisset Llano and Shannon Czorny.

The fourth chapter of this thesis describes potential future directions and initial work towards an inverse-electron demand Diels-Alder approach to trigger the release of Ga/^{67}GaDFO as dual therapeutic and imaging agents. Precursors as described in the chapter were synthesized and characterized by the author.

References

(1) Bleeker-Rovers, C. P.; Vos, F. J.; Van Der Graaf, W. T. A.; Oyen, W. J. G. *Oncologist* **2011**, *16*, 980-991.

(2) Thomson, P. D.; Smith, D. J. *Am. J. Surg.* **1994**, *167*, S7–S11.

(3) Pendleton, J. N.; Gorman, S. P.; Gilmore, B. F., *Expert Review of Anti-infective Therapy*, **2013**, *11*, 297-308.

(4) Budin, G.; Chung, H. J.; Lee, H.; Weissleder, R. *Angew. Chem. Int. Ed. Engl.* **2012**, *51*, 7752–7755.

(5) Coico, R. *Curr. Protoc. Immunol.* **2001**, A – 3O.

(6) Costerton, J. W.; Stewart, P. S.; Greenberg, E. P. *Science (80-.).* **1999**, *284*, 1318–1322.

(7) Iikuni, Y.; Okada, J.; Kondo, H; Kashiwazaki, S. *Internal Medicine* **1994**, *33*, 67-73.

(8) Arnow, P. M.; Flaherty, J. P. *Lancet* **1997**, *350*, 575–580.

(9) Busse, P. J.; Mathur, S. K. *J. Allergy Clin. Immunol.* **2010**, *126*, 690–699.

(10) Asquith, M.; Haberthur, K.; Brown, M.; Engelmann, F.; Murphy, A.; Al-Mahdi, Z.; Messaoudi, I. *Pathobiol. Aging Age Relat. Dis.* **2012**, *2*.

(11) van Oosten, M.; Schäfer, T.; Gazendam, J. a C.; Ohlsen, K.; Tsompanidou, E.; de Goffau, M. C.; Harmsen, H. J. M.; Crane, L. M. a; Lim, E.; Francis, K. P.; Cheung, L.; Olive, M.; Ntziachristos, V.; van Dijl, J. M.; van Dam, G. M. *Nat. Commun.* **2013**, *4*, 2584.

(12) Wolcott, R.; Dowd, S. *Plast. Reconstr. Surg.* **2011**, *127*, 28S – 35S.

(13) Costerton, J. W.; Montanaro, L.; Arciola, C. R. *Int. J. Artif. Organs* **2005**, *28*, 1062–1068.

(14) Zimmerli, W.; Trampuz, A. In *Biomaterials Associated Infection*; Springer, 2013; 3–24.

(15) Karlowsky, J. A.; Jones, M. E.; Draghi, D. C.; Thornsberry, C.; Sahm, D. F.; Volturo, G. A. *Ann. Clin. Microbiol. Antimicrob.* **2004**, *3*, 7.

(16) Toone, E. *Adv. Enzym. Relat. Areas Mol. Biol.* **2011**, *77*, 11–13.

(17) Bunschoten, a; Welling, M. M.; Termaat, M. F.; Sathekge, M.; van Leeuwen, F. W. B. *Bioconjug. Chem.* **2013**, *24*, 1971–1989.

(18) Signore, A.; Mather, S. J.; Piaggio, G.; Malviya, G.; Dierckx, R. A. *Chem. Rev.* **2010**, *110*, 3112–3145.

(19) Saha, G. B. *Fundamentals of Nuclear Pharmacy*; 2004.

(20) Kumar, V.; K Boddeti, D.; G Evans, S.; Angelides, S. *Curr. Radiopharm.* **2012**, *5*, 71–75.

(21) Ning, X.; Seo, W.; Lee, S.; Takemiya, K.; Rafi, M.; Feng, X.; Weiss, D.; Wang, X.; Williams, L.; Camp, V. M. *Angew. Chemie* **2014**, *126*, 14320–14325.

(22) Weinstein, E. A.; Ordonez, A. A.; DeMarco, V. P.; Murawski, A. M.; Pokkali, S.; MacDonald, E. M.; Klunk, M.; Mease, R. C.; Pomper, M. G.; Jain, S. K. *Sci. Transl. Med.* **2014**, *6*, 259ra146–ra259ra146.

(23) Sugawara, Y.; Gutowski, T. D.; Fisher, S. J.; Brown, R. S.; Wahl, R. L. *Eur. J. Nucl. Med.* **1999**, *26*, 333–341.

(24) F. De Winter, D. Vogelaers, F. G. *Eur J Clin Microbiol Infect Dis* **2002**, *21*, 247–257.

(25) Nicolas Dumarey, Dominique Egrise, Didier Blocklet, Bernard Stallenberg, Myriam Remmelink, Veronique del Marmol, Gaetan Van Simaeys, Frederique Jacobs, S. G. *J Nucl Med* **2006**, *47*, 625–632.

(26) van Dam, G. M.; Themelis, G.; Crane, L. M. a; Harlaar, N. J.; Pleijhuis, R. G.; Kelder, W.; Sarantopoulos, A.; de Jong, J. S.; Arts, H. J. G.; van der Zee, A. G. J.; Bart, J.; Low, P. S.; Ntziachristos, V. *Nat. Med.* **2011**, *17*, 1315–1319.

(27) Ning, X.; Lee, S.; Wang, Z.; Kim, D.; Stubblefield, B.; Gilbert, E.; Murthy, N.

Nat. Mater. **2011**, *10*, 602–607.

(28) Ntziachristos, V. *Nat. Methods* **2010**, *7*, 603–614.

(29) Issadore, D.; Shao, H.; Chung, J.; Newton, A.; Pittet, M.; Weissleder, R.; Lee, H. *Lab Chip* **2011**, *11*, 147–151.

(30) Chung, H. J.; Reiner, T.; Budin, G.; Min, C.; Liong, M.; Issadore, D.; Lee, H.; Weissleder, R. *ACS Nano* **2011**, *5*, 8834–8841.

(31) Hider, R. C.; Kong, X. *Nat. Prod. Rep.* **2010**, *27*, 637–657.

(32) Thulasiraman, P.; Newton, S. M. C.; Xu, Jide; Raymond, K. N.; Mai, C; Hall, A.; Montague, M. A.; Klebba, P. E. *J. Bacteriol.* **1998**, *180*, 6689-6696.

(33) Zhai, C.; Summer, D.; Rangger, C.; Haas, H.; Haubner, R.; Decristoforo, C. *J. Label. Compd. Radiopharm.* **2015**, *58*, 209–214.

(34) Petrik, M.; Haas, H.; Schrettl, M.; Helbok, A.; Blatzer, M.; Decristoforo, C. *Nucl. Med. Biol.* **2012**, *39*, 361–369.

(35) Petrik, M.; Franssen, G. M.; Haas, H.; Laverman, P.; Hörtnagl, C.; Schrettl, M.; Helbok, A.; Lass-Flörl, C.; Decristoforo, C. *Eur. J. Nucl. Med. Mol. Imaging* **2012**, *39*, 1175–1183.

(36) Petrik, M.; Haas, H.; Dobrozemsky, G.; Lass-Flörl, C.; Helbok, A.; Blatzer, M.; Dietrich, H.; Decristoforo, C. *J. Nucl. Med.* **2010**, *51*, 639–645.

(37) Knetsch, P. A.; Zhai, C.; Rangger, C.; Blatzer, M.; Haas, H.; Kaeopookum, P.; Haubner, R.; Decristoforo, C. *Nucl. Med. Biol.* **2015**, *42*, 115–122.

(38) Yokoyama, A.; Ohmomo, Y.; Horiuchi, K.; Saji, H.; Tanaka, H.; Yamamoto, K.; Ishii, Y.; Torizuka, K. *J. Nucl. Med. Off. Publ. Soc. Nucl. Med.* **1982**, *23*, 909–914.

(39) Neilands, J. B. *Ann. Rev. Biochem.* **1981**, *50*, 715–731.

(40) Banin, E.; Lozinski, A.; Brady, K. M.; Berenshtein, E.; Butterfield, P. W.; Moshe, M.; Chevion, M.; Greenberg, E. P.; Banin, E. *Proc. Natl. Acad. Sci.* **2008**, *105*, 16761–16766.

(41) Larikka, M. J.; Ahonen, A. K.; Niemelä, O.; Puronto, O.; Junila, J. A.; Hämäläinen, M. M.; Britton, K.; Syrjälä, H. P. *Nucl. Med. Commun.* **2002**, *23*, 167–170.

(42) De Winter, F.; Gemmel, F.; Van Laere, K.; De Winter, O.; Poffijn, B.; Dierckx, R. A.; Van de Wiele, C. *Eur. J. Nucl. Med. Mol. Imaging* **2004**, *31*, 233–239.

(43) Vinjamuri, S.; Solanki, K. K.; Bomanji, J.; Siraj, Q.; Britton, K. E.; Hall, A. V; O'Shaughnessy, E.; Das, S. S. *Lancet* **1996**, *347*, 233–235.

(44) Sarda, L.; Crémieux, A.-C.; Lebellec, Y.; Meulemans, A.; Lebtahi, R.; Hayem, G.; Génin, R.; Delahaye, N.; Huten, D.; Le Guludec, D. *J. Nucl. Med.* **2003**, *44*, 920–926.

(45) Dumarey, N.; Blocklet, D.; Appelboom, T.; Tant, L.; Schoutens, A. *Eur. J. Nucl. Med. Mol. Imaging* **2002**, *29*, 530–535.

(46) Oyen, W. J. G.; Corstens, F. H. M.; Boerman, O. C. *Eur. J. Nucl. Med. Mol. Imaging* **2005**, *32*, 151–152.

(47) Chattopadhyay, S.; Ghosh, M.; Sett, S.; Das, M. K.; Chandra, S.; De, K.; Mishra,

M.; Sinha, S.; Sarkar, B. R.; Ganguly, S. *Appl. Radiat. Isot.* **2012**, *70*, 2384–2387.

(48) Diniz, S. O. F.; Rezende, C. M. F.; Serakides, R.; Ferreira, R. L. B.; Ribeiro, T. G.; Martin-Comin, J.; Cardoso, V. N. *Nucl. Med. Commun.* **2008**, *29*, 830–836.

(49) Lambrecht, F. Y.; Durkan, K.; Unak, P. *J. Radioanal. Nucl. Chem.* **2008**, *275*, 161–164.

(50) Mostafa, M.; Motaleb, M. A.; Sakr, T. M. *Appl. Radiat. Isot.* **2010**, *68*, 1959–1963.

(51) Motaleb, M. *J. Radioanal. Nucl. Chem.* **2007**, *272*, 167–171.

(52) Ercan, M. T.; Aras, T.; Ünsal, I. S. *Int. J. Radiat. Appl. instrumentation. Part B. Nucl. Med. Biol.* **1992**, *19*, 803–806.

(53) Roohi, S.; Mushtaq, A.; Jehangir, M.; Malik, S. A. *J. Radioanal. Nucl. Chem.* **2006**, *267*, 561–566.

(54) Tsopelas, C.; Penglis, S.; Ruszkiewicz, A.; Bartholomeusz, F. D. L. *Nucl. Med. Biol.* **2003**, *30*, 169–175.

(55) Perkins, H. R.; Nieto, M. *Biochem. J* **1970**, *116*, 83–92.

(56) Roohi, S.; Mushtaq, A.; Malik, S. A. *Radiochim. Acta* **2005**, *93*, 415–418.

(57) Jalilian, A. R.; Hosseini, M. A.; Majdabadi, A.; Saddadi, F. *Nucl. Med. Rev.* **2008**, *11*, 1–4.

(58) Halder, K. K.; Nayak, D. K.; Baishya, R.; Sarkar, B. R.; Sinha, S.; Ganguly, S.; Debnath, M. C. *Metallomics* **2011**, *3*, 1041–1048.

(59) Ocakoglu, K.; Bayrak, E.; Onursal, M.; Yilmaz, O.; Lambrecht, F. Y.; Holzwarth,

A. R. *Appl. Radiat. Isot.* **2011**, *69*, 1165–1168.

(60) Rossouw, D. D.; Lötter, M. G.; du Raan, H.; Jansen, S. E.; Höhn, A.; Burger, B. V. *Nucl. Med. Biol.* **2005**, *32*, 385–394.

(61) Shah, S. Q.; Khan, A. U.; Khan, M. R. *Appl. Radiat. Isot.* **2010**, *68*, 2255–2260.

(62) Wong, E.; Fauconnier, T.; Nguyen, T.; Pollak, A.; Rakhit, S. Glycopeptide-chelator conjugates, 2000.

(63) Leblond, F.; Davis, S. C.; Valdés, P. A.; Pogue, B. W. *J. Photochem. Photobiol. B Biol.* **2010**, *98*, 77–94.

Chapter 2

Synopsis

The work discussed in chapter 2 is prepared for submission to the journal of Nuclear Medicine and Biology. This work was done in collaboration with Dr. Joseph Ioppolo. My contributions to the work were to synthesize and characterize DFO-*n*-hexyl, DFO-*n*-quinoline, DFO-*n*-hexyl carbamate, and DFO-*n*-hexylamine-Boc carbamate, and DFO-*n*-hexylamine carbamate derivatives and their respective metal ligands. Furthermore, I prepared the radiometal complexes of all DFO ligands described herein. Moreover, I helped prepare the final manuscript. The biological studies were done by Megan Blacker while the cell uptake studies were done by Lisset Llano and Deanna Caldwell.

2 Abstract: Preparation and screening of gallium-67 labelled deferoxamine derivatives for imaging bacterial infections

Introduction: Current techniques used to detect and diagnose bacterial infections have critical limitations and an active search for improved *in vivo* imaging strategies remains. One new approach is to prepare radiolabelled siderophores, such as ^{67}Ga-deferoxamine (DFO), as analogues of the corresponding iron complexes that are actively and selectively taken up by bacteria. Unfortunately simple [$^{67/68}$Ga]-DFO derivatives clear too rapidly and do not effectively target sites of infection *in vivo*. We investigated whether

DFO derivatives with altered pharmacokinetic properties would still be actively transported via the bacterial iron sequestering pathway.

Methods: A library of DFO derivatives were synthesized by functionalizing the terminal amine of DFO, using two convenient carbamate-forming reactions. The corresponding ^{67}Ga labelled complexes were prepared and their uptake in *S. aureus* assessed *in vitro*. Biodistribution studies on lead compounds were performed in a murine infection model.

Results: ^{67}Ga-DFO derivatives containing alkyl, aromatic or H-bonding substituents were prepared and isolated in > 90% radiochemical yield and > 95% radiochemical purity. Bacterial uptake studies *in vitro* versus DFO revealed that both compounds had comparable uptake after 24 hours. Blocking studies, using non-radioactive Ga-DFO showed that the uptake was specific transport via the iron-sequestering pathway. Biodistribution studies with an ethyl carbamate-DFO derivative in mice with S. aureus infection in one thigh showed good infected-to-non-infected thigh ratios (11:1), but high non-specific binding in the GI tract.

Conclusion: The work reported shows that it is possible to functionalize DFO-type siderophores and retain active uptake of the ^{67}Ga-labelled complexes, by bacteria.

Advances in Knowledge and Implications for Patient Care: We have shown that it is possible to modify DFO and retain the ability of the corresponding ^{67}Ga complexes to be taken up by bacteria via the siderophore iron-sequestering pathway. This new knowledge suggests that it is possible to develop siderophore-based tracers for imaging infection by targeting a pathway that is unique to bacteria.

2.1 Introduction

Bacterial infection and antibiotic resistance are global healthcare issues requiring rapid and accurate diagnosis of infection [1,2]. Nuclear medicine techniques are used extensively to image infections, with radiolabelled leukocytes as the predominant diagnostic agent [3,4]. However, this technique is time consuming and creates an infection hazard to health care providers as well as patients, because blood must be drawn, separated, labelled and re-injected. Alternative techniques include the use of ^{67}Ga-citrate and ^{18}F-2-fluorodeoxyglucose (^{18}F-FDG) [1]. However both of these radiopharmaceuticals show poor specificity for infection, because they can also image tumours and sites of inflammation or elevated glucose metabolism [1,5,6]. In light of these limitations, there is an active search for new radiopharmaceuticals for imaging infection [7–10].

One approach is to exploit the mechanism by which bacteria recruit iron from their environment. Iron is a limiting nutrient for bacteria because human iron-scavenging proteins maintain free Fe^{3+} concentrations in tissues and blood at extremely low levels ($\approx 10^{-24}$ M) [11]. In response, bacteria produce siderophores, which are small molecules designed to scavenge iron. Siderophores have exceptionally high affinity for Fe^{3+} (some with $K_a = 10^{49}$ M^{-1}), allowing bacteria to selectively bind the metal and actively transport the resulting complex. Ga^{3+} has ionic radii similar to Fe^{3+}, and these metals have similar coordination chemistry and ligand preferences [12]. Consequently, gallium radioisotope complexes, notably those containing ^{67}Ga and ^{68}Ga, can be used as Fe-siderophore mimetics [13]. The ^{67}Ga analogue of ferrichrome for example was shown to be taken up

by the fungus *Ustilago sphaerogena*, via an active mechanism that was indistinguishable from ferrichrome [14]. Decristoforo *et al.* prepared ^{68}Ga complexes form a series of siderophores, to use as tools to detect invasive pulmonary aspergillosis, caused by *A. fumigatus;* a common airborne fungi [15]. In a rat infection model, uptake into focal infection sites in the lung was detected using micro PET studies [15].

Of the siderophores available that could be used for bacterial rather than fungal imaging, deferoxamine (desferrioxamine B, DFO) is one of the most attractive, because it is used by a wide variety of bacterial species to sequester iron. It is also approved for use as a pharmaceutical for iron chelation therapy, and its non-radioactive Ga complex was shown to have potential to enhance anti-pseudomonas treatments [16]. Unfortunately, the gallium complex of DFO is excreted rapidly, as demonstrated by the prompt accumulation of ^{68}Ga-DFO in the bladder and nearly complete eliminated within 10 min, in healthy mice [17,18]. The suboptimal pharmacokinetics limits the utility of ^{68}Ga-DFO as a diagnostic agent, and modification of the core structure would be necessary to develop a viable radiopharmaceutical for imaging infection. One possible approach is to derivatize DFO, including neutralizing the charge of the pendent amine group, to modify the clearance route and kinetics. What remains unknown with this approach is the impact of the substitution on the extent of active transport of the corresponding ^{67}Ga-DFO complexes by bacteria. To answer this question, a library of alkyl and aryl DFO derivatives was prepared, and their ^{67}Ga complexed derivatives were generated, in order to determine if functionalized forms of the chelate-metal complex would still be taken up by the bacterial iron-sequestering pathway.

2.2 Materials and Methods

2.2.1 Materials and Instrumentation.

Deferoxamine mesylate **1** was purchased from Santa Cruz, USA. All solvents and reagents were purchased from Sigma-Aldrich and Bioshop Canada (Burlington, ON), unless otherwise noted, and were used without further purification. Water purified by reverse osmosis was used for all non-radioactive experiments requiring water. Compounds **13** and **16** and *t*-butyl-(6-(((4-nitrophenoxy)carbonyl)oxy)hexyl)carbamate were prepared according to literature procedures [19-21]. For radiochemistry experiments, high purity concentrated HCl (35% (*w/v*), 99.999% trace metal analysis (Sigma-Aldrich) and ultra-pure water (Millipore Direct-Q3) were used to prepare the required solutions. $^{67}GaCl_3$ in 0.1 M HCl was purchased from Nordion Inc. (Vancouver, Canada).

^{1}H and ^{13}C nuclear magnetic resonance (NMR) spectra were recorded on a Bruker Avance 600 instrument (^{1}H: 600 MHz, ^{13}C: 151 MHz) at 300 K. NMR chemical shifts (δ) are reported in ppm and coupling constants expressed in Hz. ^{1}H and ^{13}C NMR spectra were referenced to residual solvent peaks. IR spectra were recorded on a Nicolet 6700 FT-IR spectrometer. High-resolution ESI mass spectra were collected on a Waters Micromass Global Q-TOF Ultima mass spectrometer. Melting points were determined using a Gallenkamp melting point apparatus and are uncorrected. Analytical HPLC was performed on an Agilent 1100 system equipped with an autosampler, a variable wavelength UV detector and Bioscan gamma detector connected in series. A

Phenomenex Gemini column (5 µm, 4.6 × 250 mm, C18) fitted with a guard column was used, employing 0.01 M NH_4OAc in H_2O and neat MeCN as mobile phases at a flow rate of 1 mL/min. Radiochemical purity was determined by an integration of peaks in the HPLC γ-trace, and the identity of each radiolabelled product was confirmed by co-injection with the appropriate non-radioactive ("cold") gallium analogue. Semi-preparative HPLC was performed on a Varian Pro-Star system using a Phenomenex Jupiter C4 column (260 × 10 mm, 5 µm, 300 Å) fitted with a guard column at a flow rate of 4 mL/min. Preparative HPLC was performed on an Agilent 1200 system using a Phenomenex Gemini-NX column (250 × 21.2 mm, 5µm, 100 Å) fitted with a guard column at a flow rate of 20 mL/min. Preparative, semi-preparative and analytical HPLC were performed using acetonitrile and water in the following gradients: Method A: 0−5 min 10% MeCN, 5−20 min 10−60% MeCN, 20−22 min 60% MeCN, 22−23 min 60−10% MeCN, 23−30 min 10% MeCN. Method B: 0−5 min 5% MeCN, 5−20 min 5−60% MeCN, 20−22 min 60% MeCN, 22−23 min 60−5% MeCN, 23−30 min 5% MeCN. Method C: 0−5 min 10% MeCN, 5−20 min 10−50% MeCN, 20−22 min 50% MeCN, 22−23 min 50−10% MeCN, 23−30 min 10% MeCN.

2.2.2 Chemical Synthesis:

2.2.2.1 General procedure for preparation of 2-7 and 9

A solution of DFO (**1**) and i-Pr2EtN (1:2 mol ratio) in DMF (2 mL) was prepared with stirring at 90 °C. The required alkyl chloroformate (1 eq.) was then added in one

portion and the solution stirred at 90 °C overnight. The desired product was isolated by semi-preparative or preparative HPLC (elution method A). Following concentration to dryness, the resulting residue was re-suspended in MeCN (5 mL), filtered, and the residue washed with H2O (3 × 1 mL). The isolated material was dried under vacuum filtration as a colourless solid.

2.2.2.2 **Deferoxamine methyl carbamate (2)**

Compound **2** was prepared from **1** (102 mg, 0.15 mmol) according to the general procedure in 38% yield (36 mg, 0.058 mmol). ^{1}H NMR (600 MHz, DMSO-d_6) δ 9.61 (br m, 3H), 7.77 (br m, 2H), 7.01 (br m, 1H), 3.50 (s, 3H), 3.45 (m, 6H), 3.00 (m, 4H), 2.93 (m, 2H), 2.57 (m, 4H), 2.27 (m, 4H), 1.96 (s, 3H), 1.49 (m, 6H), 1.38 (m, 6H), 1.21 (m, 6H); ^{13}C NMR (150 MHz, DMSO-d_6) δ 172.0, 172.0, 171.3, 171.3, 170.1, 156.7, 51.1, 47.1, 47.1, 46.8, 40.2, 38.4, 38.4, 29.9, 29.9, 29.1, 28.8, 28.8, 27.6, 27.6, 26.0, 26.0, 26.0, 23.5, 23.5, 23.4, 20.3; IR (KBr pellet) 3432, 3309, 2930, 2857, 1693, 1621, 1564 cm^{-1}; HRMS-ESI (m/z): $[M+H]^+$ calcd for $C_{27}H_{51}N_6O_{10}$: 619.3667, absd 619.3666. t_R (Method B) 15.9 min; M.p. 145−147 °C.

2.2.2.3 **Deferoxamine ethyl carbamate (3)**

Compound **3** was prepared from **1** (157 mg, 0.24 mmol) according to the general procedure in 43% yield (64.7 mg, 0.10 mmol). ^{1}H NMR (600 MHz, DMSO-d_6) δ 9.60 (br m, 3H), 7.76 (br m, 2H), 7.01 (br m, 1H), 3.95 (q, J = 7.1 Hz, 2H), 3.45 (m, 6H), 3.00 (m, 4H), 2.93 (m, 2H), 2.57 (m, 4H), 2.26 (m, 4H), 1.93 (s, 3H), 1.49 (m, 6H), 1.38 (m, 6H), 1.21 (m, 6H), 1.14 (t, J = 7.1 Hz, 3H); ^{13}C NMR (150 MHz, DMSO-d_6) δ 172.0, 172.0,

171.3, 171.3, 170.1, 156.2, 59.4, 47.1, 47.1, 46.8, 40.0, 38.4, 38.4, 29.9, 29.9, 29.1, 28.8, 28.8, 27.6, 27.6, 26.0, 26.0, 26.0, 23.5, 23.5, 23.4, 20.4, 14.7; IR (KBr pellet) 3311, 3148, 2930, 2857, 1688, 1622, 1565 cm^{-1}; HRMS-ESI (m/z): $[M+H]^+$ calcd for $C_{28}H_{53}N_6O_{10}$: 633.3823, obsd 633.3813. t_R (Method B) 16.7 min; M.p. 153−155 °C.

2.2.2.4 Deferoxamine *n*-propyl carbamate (4)

Compound **4** was prepared from **1** (148 mg, 0.23 mmol) according to the general procedure in 37% yield (54.7 mg, 0.085 mmol). ^1H NMR (600 MHz, DMSO-d_6) δ 9.59 (br m, 3H), 7.76 (br m, 2H), 7.02 (br m, 1H), 3.86 (t, J = 6.6 Hz, 2H), 3.45 (m, 6H), 3.00 (m, 4H), 2.96 (m, 2H), 2.57 (m, 4H), 2.27 (m, 4H), 1.96 (s, 3H), 1.54 (m, 2H), 1.49 (m, 6H), 1.38 (m, 6H), 1.21 (m, 6H), 0.86 (t, J = 7.5 Hz, 3H); ^{13}C NMR (150 MHz, DMSO-d_6) δ 172.0, 172.0, 171.3, 171.3, 170.1, 156.3, 65.0, 47.1, 47.1, 46.8, 40.1, 38.4, 38.4, 29.9, 29.9, 29.1, 28.8, 28.8, 27.6, 27.6, 26.0, 26.0, 26.0, 23.5, 23.5, 23.4, 22.1, 20.3, 10.3; IR (KBr pellet) 3430, 3322, 3131, 2931, 2863, 1687, 1650, 1623, 1597 cm^{-1}; HRMS-ESI (m/z): $[M+H]^+$ calcd for $C_{29}H_{55}N_6O_{10}$: 647.3980, obsd 647.3976. t_R (Method B) 19.5 min; M.p. 147−150 °C.

2.2.2.5 Deferoxamine *i*-propyl carbamate (5)

Compound **5** was prepared from **1** (197 mg, 0.30 mmol) according to the general procedure in 30% yield (59 mg, 0.091 mmol). ^1H NMR (600 MHz, DMSO-d_6) δ 9.63 (br m, 1H), 9.59 (br m, 2H), 7.76 (br m, 2H), 6.94 (br m, 1H), 4.72 (m, 1H), 3.45 (m, 6H), 3.00 (m, 4H), 2.92 (m, 2H), 2.57 (m, 4H), 2.27 (m, 4H), 1.96 (s, 3H), 1.49 (m, 6H), 1.38 (m, 6H), 1.21 (m, 6H), 1.14 (d, J = 6.0 Hz, 6H); ^{13}C NMR (150 MHz, DMSO-d_6) δ 172.0,

172.0, 171.3, 171.3, 170.1, 155.9, 66.4, 47.1, 47.1, 46.8, 40.0, 38.4, 38.4, 29.9, 29.9, 29.1, 28.8, 28.8, 27.6, 27.6, 26.0, 26.0, 26.0, 23.5, 23.5, 23.4, 22.1, 20.3; IR (KBr pellet) 3311, 2930, 2859, 1684, 1621, 1564 cm^{-1}; HRMS-ESI (m/z): $[M+H]^+$ calcd for $C_{29}H_{55}N_6O_{10}$: 647.3980, obsd 647.3978. t_R (Method B) 17.5 min; M.p. 143−145 °C.

2.2.2.6 Deferoxamine *n*-butyl carbamate (6)

Compound **6** was prepared from **1** (164 mg, 0.25 mmol) according to the general procedure in 30% yield (49 mg, 0.074 mmol). ^1H NMR (600 MHz, DMSO-d_6) δ 9.60 (br m, 3H), 7.76 (br m, 2H), 7.01 (br m, 1H), 3.91 (t, J = 6.9 Hz, 2H), 3.44 (m, 6H), 3.00 (m, 4H), 2.93 (m, 2H), 2.57 (m, 4H), 2.27 (m, 4H), 1.96 (s, 3H), 1.49 (m, 8H), 1.38 (m, 6H), 1.31 (m, 2H), 1.21 (m, 6H), 0.88 (t, J = 7.2 Hz, 3H); ^{13}C NMR (150 MHz, DMSO-d_6) δ 172.0, 172.0, 171.3, 171.3, 170.1, 156.3, 63.2, 47.1, 47.1, 46.8, 40.1, 38.4, 38.4, 30.8, 29.9, 29.9, 29.1, 28.8, 28.8, 27.6, 27.6, 26.0, 26.0, 26.0, 23.5, 23.5, 23.3, 20.3, 18.6, 13.6; IR (KBr pellet) 3322, 3130, 2932, 2864, 1686, 1652, 1623, 1597 cm^{-1}; HRMS-ESI (m/z): $[M+H]^+$ calcd for $C_{30}H_{57}N_6O_{10}$: 661.4136, obsd 661.4133. t_R (Method B) 18.6 min; M.p. 153 °C.

2.2.2.7 Deferoxamine *i*-butyl carbamate (7)

Compound **7** was prepared from **1** (229 mg, 0.35 mmol) according to the general procedure in 35% yield (81 mg, 0.12 mmol). ^1H NMR (600 MHz, DMSO-d_6) δ 9.60 (br m, 3H), 7.76 (br m, 2H), 7.03 (br m, 1H), 3.70 (d, J = 6.6 Hz, 2H), 3.45 (m, 6H), 3.00 (m, 4H), 2.94 (m, 2H), 2.57 (m, 4H), 2.27 (m, 4H), 1.96 (s, 3H), 1.81 (m, 1H), 1.49 (m, 6H), 1.38 (m, 6H), 1.21 (m, 6H), 0.86 (d, J = 6.6 Hz, 6H); ^{13}C NMR (150 MHz, DMSO-d_6) δ

172.0, 172.0, 171.3, 171.3, 170.1, 156.4, 69.6, 47.1, 47.1, 46.8, 40.1, 38.4, 38.4, 29.9, 29.9, 29.1, 28.8, 28.8, 27.7, 27.6, 27.6 26.0, 26.0, 26.0, 23.5, 23.5, 23.3, 20.3, 18.9; IR (KBr pellet) 3323, 3131, 2944, 2864, 1686, 1651, 1624, 1598 cm^{-1}; HRMS-ESI (m/z): $[M+H]^+$ calcd for $C_{30}H_{57}N_6O_{10}$: 661.4136, obsd 661.4146. t_R (Method B) 18.5 min; M.p. 152 °C.

2.2.2.8 Deferoxamine Boc (8)

Compound **8** was produced using a published protocol [22]. A solution of **1** (157 mg, 0.24 mmol) and *i*-Pr_2EtN (83.3 μL, 0.48 mmol) in DMF (2 mL) was prepared by stirring at 90 °C. Then, a solution of Boc_2O (67.9 mg, 0.31 mmol) in DMF (2 mL) was added in one portion and the mixture stirred at this temperature for 18.5 h. The solvent was removed by rotary evaporation and the residue that remained was suspended in chilled MeCN (20 mL). The insoluble material was collected by filtration, washed with MeCN (3 × 1 mL) and air-dried under vacuum filtration to obtain **8** in 92% yield as a colourless powder (146 mg, 0.22 mmol). ^1H NMR (600 MHz, DMSO-d_6) δ 9.63 (br m, 1H), 9.59 (br m, 2H), 7.76 (br m, 2H), 6.74 (br m, 1H), 3.45 (m, 6H), 3.00 (m, 4H), 2.87 (m, 2H), 2.57 (m, 4H), 2.27 (m, 4H), 1.96 (s, 3H), 1.49 (m, 6H), 1.39 (m, 6H), 1.36 (s, 9H), 1.21 (m, 6H); ^{13}C NMR (150 MHz, DMSO-d_6) δ 172.0, 172.0, 171.3, 171.3, 170.1, 155.6, 77.3, 47.1, 47.1, 46.8, 39.7, 38.4, 38.4, 29.9, 29.9, 29.1, 28.8, 28.8, 28.3, 27.6, 27.6, 26.0, 26.0, 26.0, 23.5, 23.5, 23.4, 20.3; IR (KBr pellet) 3368, 3322, 3145, 2934, 2863, 1688, 1652, 1626, 1603 cm^{-1}; HRMS-ESI (m/z): $[M+H]^+$ calcd for $C_{30}H_{57}N_6O_{10}$: 661.4136, obsd 661.4138. t_R (Method B) 18.3 min; M.p. 124 °C.

2.2.2.9 Deferoxamine *n*-hexyl carbamate (9)

Compound **9** was prepared from **1** (149 mg, 0.23 mmol) according to the general procedure in 38% yield (60 mg, 0.087 mmol). ^{1}H NMR (600 MHz, DMSO-d_6) δ 9.60 (br m, 3H), 7.76 (br m, 2H), 7.01 (br m, 1H), 3.90 (t, J = 6.6 Hz, 2H), 3.45 (m, 6H), 3.00 (m, 4H), 2.93 (m, 2H), 2.57 (m, 4H), 2.27 (m, 4H), 1.96 (s, 3H), 1.49 (m, 8H), 1.38 (m, 6H), 1.26 (m, 6H), 1.21 (m, 6H), 0.86 (t, J = 6.9 Hz, 3H); ^{13}C NMR (150 MHz, DMSO-d_6) δ 172.0, 172.0, 171.3, 171.3, 170.1, 156.3, 63.5, 47.1, 47.1, 46.8, 40.1, 38.4, 38.4, 30.9, 29.9, 29.9, 29.1, 28.8, 28.8, 28.7, 27.6, 27.6, 26.0, 26.0, 26.0, 25.0, 23.5, 23.5, 23.3, 22.0, 20.3, 13.9; IR (KBr pellet) 3433, 3321, 3133, 2931, 2863, 1686, 1651, 1624, 1598 cm^{-1}; HRMS-ESI (m/z): $[M+H]^+$ calcd for $C_{32}H_{61}N_6O_{10}$: 689.4449, obsd 689.4464. t_R (Method B) 20.6 min; M.p. 154 °C.

2.2.2.10 Deferoxamine *n*-hexylamine-Boc carbamate (10)

A solution of **1** (354 mg, 0.54 mmol) and *i*-Pr_2EtN (188 μL, 1.1 mmol) in DMF (5 mL) was prepared by stirring at 90 °C. *t*-Butyl-(6-(((4-nitrophenoxy)carbonyl)oxy)hexyl)carbamate [19] (227 mg, 0.59 mmol) was then added in one portion and the solution stirred at this temperature overnight. The mixture was allowed to cool to room temperature and purified by preparative HPLC to obtain **10** in 74% yield as a colourless powder (320 mg, 0.40 mmol). ^{1}H NMR (600 MHz, DMSO-d_6) δ 9.60 (br m, 3H), 7.76 (br m, 2H), 7.01 (br m, 1H), 6.74 (br m, 1H), 3.89 (t, J = 6.7, 2H), 3.45 (m, 6H), 3.00 (m, 4H), 2.93 (m, 2H), 2.88 (m, 2H), 2.57 (m, 4H), 2.26 (m, 4H), 1.96 (s, 3H), 1.49 (m, 8H), 1.38 (m, 8H), 1.36 (s, 9H), 1.22 (m, 10H); ^{13}C NMR (150 MHz,

DMSO-d_6) δ 172.0, 172.0, 171.3, 171.3, 170.1, 156.3, 155.6, 63.5, 77.3, 47.1, 47.1, 46.8, 40.1, 39.8, 38.4, 38.4, 29.9, 29.9, 29.4, 29.1, 28.8, 28.8, 28.7, 28.3, 27.6, 27.6, 26.0, 26.0, 26.0, 26.0, 25.1, 23.5, 23.5, 23.3, 20.3; IR (KBr pellet) 3323, 3134, 2931, 2863, 1689, 1652, 1624, 1598 cm^{-1}; HRMS-ESI (m/z): $[M+H]^+$ calcd for $C_{37}H_{70}N_7O_{12}$: 804.5082, obsd 804.5059. t_R (Method B) 20.7 min; M.p. 145 °C.

2.2.2.11 Deferoxamine *n*-hexylamine carbamate (11)

To a stirred solution of **10** (72.0 mg, 0.090 mmol) in DMSO (3.4 mL) at room temperature was added concentrated phosphoric acid (85%, 3.4 mL). The mixture was stirred for 1.5 h. An additional portion of phosphoric acid was added (85%, 3.4 mL) and the mixture stirred at room temperature for an additional 1.5 h. The mixture was diluted to 500 mL with water and then passed through a Waters C18 Sep-Pak cartridge. The cartridge was washed with water (30 mL) and the product eluted with MeOH (30 mL). The MeOH solvent was partially removed by rotary evaporation (ca. 2 mL remaining) then triturated with chilled Et_2O (5 mL). The fine precipitate that formed was collected by filtration and air-dried under vacuum filtration to obtain **11** in 58% yield as an off-white powder (37 mg, 0.052 mmol). ^{1}H NMR (600 MHz, DMSO-d_6) δ 7.82 (br m, 2H), 7.03 (br m, 1H), 3.91 (m, 2H), 3.45 (m, 6H), 2.99 (m, 4H), 2.93 (m, 2H), 2.61 (br m, 2H), 2.57 (m, 4H), 2.27 (m, 4H), 1.96 (s, 3H), 1.49 (m, 8H), 1.44 (m, 2H), 1.38 (m 6H), 1.28 (m, 4H), 1.21 (m, 6H) (NOH and NH_2 not observed); ^{13}C NMR (150 MHz, DMSO-d_6) δ 171.9, 171.9, 171.3, 171.3, 170.1, 156.3, 63.4, 47.1, 47.1, 46.8, 40.1, 39.9, 38.4, 38.4, 30.0, 30.0, 29.6, 29.1, 28.8, 28.8, 28.7, 27.6, 27.6, 26.0, 26.0, 26.0, 25.9, 25.2, 23.5, 23.5, 23.4, 20.3; IR (KBr pellet) 3429, 3309, 2930, 2857, 1689, 1621, 1566 cm^{-1}; HRMS-ESI

(m/z): $[M+H]^+$ calcd for $C_{32}H_{62}N_7O_{10}$: 704.4558, obsd 704.4526. t_R (Method B) 15.9 min; M.p. >205 °C (decomp.).

2.2.2.12 Deferoxamine Cbz (12)

Compound **12** was produced using a published protocol [23]. A solution of **1** (55.2 mg, 0.084 mmol) and i-Pr_2EtN (29 μL, 0.48 mmol) in DMF (2 mL) was prepared by stirring at 90 °C. Then, benzyl 4-nitrophenyl carbonate (25 mg, 0.092 mmol) was added in one portion and the solution stirred at this temperature for 24 h. The solvent was removed by rotary evaporation and the residue that remained was resuspended in MeCN (1 mL). The insoluble material was collected by filtration, washed with MeCN (3 × 1 mL) dried by vacuum filtration to obtain **12** in 93% yield as a colourless powder (51 mg, 0.078 mmol). ^{1}H NMR (600 MHz, DMSO-d_6) δ 9.63 (br m, 1H), 9.59 (br m, 2H), 7.76 (br m, 2H), 7.34 (m, 4H), 7.30 (m, 1H), 7.22 (br m, 1H), 5.00 (s, 2H), 3.45 (m, 6H), 2.99 (m, 4H), 2.96 (m, 2H), 2.57 (m, 4H), 2.27 (m, 4H), 1.96 (s, 3H), 1.49 (m, 6H), 1.38 (m, 6H), 1.21 (m, 6H); ^{13}C NMR (150 MHz, DMSO-d_6) δ 172.1, 172.1, 171.5, 171.5, 170.3, 156.2, 137.4, 128.4, 127.8, 127.8, 65.2, 47.2, 47.2, 46.9, 40.3, 38.6, 38.6, 30.0, 30.0, 29.2, 28.9, 28.9, 27.7, 27.7, 26.1, 26.1, 26.1, 23.6, 23.6, 23.5, 20.4; IR (KBr pellet) 3321, 3135, 2930, 2861, 1685, 1622 cm^{-1}; HRMS-ESI (m/z): $[M+H]^+$ calcd for $C_{33}H_{55}N_6O_{10}$: 695.3980, obsd 695.3994. t_R (Method B) 19.0 min; M.p. 133−136 °C.

2.2.2.13 Deferoxamine *N*-succinyl-*N*-ciprofloxacin (15)

Compound **15** was produced using a published protocol [24]. A solution of Ciprofloxacin (**14**) (51.7 mg, 0.16 mmol) and i-Pr_2EtN (54.4 μL, 0.31 mmol) in water (4

mL) was prepared and stirred for 15 min at room temperature. A solution of **13** (102 mg, 0.15 mmol) and PyBOP (104 mg, 0.20 mmol) in DMSO (4 mL) was prepared and the mixture stirred for 15 min at room temperature [20]. The ciprofloxacin / i-Pr_2EtN solution was added to the DFO-n-succinic acid / PyBOP solution and stirred for 1 h at 90 °C. The reaction mixture was diluted 1:10 with water and then passed through a Waters C18 Sep-Pak cartridge. The cartridge was washed with water (20 mL) and the product eluted with MeCN (20 mL). The solvent was removed to give a colourless residue which was further purified by semi-preparative HPLC to obtain **15** in 15% yield as a colourless powder (23.1 mg, 0.024 mmol). ^{1}H NMR (600 MHz, DMSO-d_6) δ 9.65 (br m, 1H), 9.61 (br m, 2H), 8.66 (s, 1H), 7.92 (m, 1H), 7.80 (m, 1H), 7.77 (m, 2H), 7.57 (m, 1H), 3.82 (m, 1H), 3.69 (m, 4H), 3.45 (m, 6H), 3.4-3.3 (br m, 4H), 3.00 (m, 6H), 2.58 (m, 6H), 2.34 (m, 2H), 2.26 (m, 4H), 1.96 (s, 3H), 1.49 (m, 6H), 1.38 (m, 6H), 1.33 (m, 2H), 1.19 (m, 6H), 1.19 (m, 2H); ^{19}F NMR (564 MHz, DMSO-d_6) δ -121.8; IR (KBr pellet) 3438, 3307, 2929, 2857, 1625, 1567, 1461 cm^{-1}; HRMS-ESI (m/z): $[M+H]^+$ calcd for $C_{46}H_{69}N_9O_{13}$: 974.4999, obsd 974.5014. t_R (Method B) 18.3 min; M.p. 170-173 °C.

2.2.3 Preparation of non-radioactive Ga complexes

2.2.3.1 General procedure for preparation of 17-28.

A 30 mM solution of the modified DFO ligand (**2-12**, **15**) (1 eq.) in DMSO or DMF was prepared. To this was added an aqueous solution of $Ga(NO_3)_3$ (30 mg/mL, 3 equiv.) in 1M sodium acetate buffer (pH 5). The solution was stirred for 30 min at 60 °C and then room temperature overnight. The mixture was diluted 10 fold with water or 1M

Na_2CO_3 (pH 9), loaded on to a Waters C18 Sep-Pak cartridge and washed with water (30 mL). The desired product was eluted with MeCN (10 mL) and the solvent was removed under a gentle stream of N_2 gas.

2.2.3.2 Ga-deferoxamine-methyl carbamate (17)

Compound **21** was prepared from **2** (15.4 mg, 0.025 mmol) using the general procedure in 88% yield (14.9 mg, 0.022 mmol). ^{1}H NMR (600 MHz, DMSO-d_6) δ 7.7-7.5 (br m, 2H), 7.08 (m, 1H), 4.0-0.9 (overl br m, 36H), 3.50 (s, 3H), 2.96 (m, 2H), 2.03 (s, 3H); IR (KBr pellet) 3432, 2931, 1705, 1652, 1594, 1555, 1458 cm^{-1}; HRMS-ESI (*m/z*): $[M+H]^+$ calcd for $C_{27}H_{48}N_6O_{10}Ga$: 685.2688, obsd 685.2691; t_R (Method B) 14.6 min.

2.2.3.3 Ga-deferoxamine-ethyl carbamate (18)

Compound **18** was prepared from **3** (17.2 mg, 0.027 mmol) using the general procedure in 94% yield (17.9 mg, 0.026 mmol). ^{1}H NMR (600 MHz, DMSO-d_6) δ 7.7-7.5 (br m, 2H), 7.03 (m, 1H), 4.0-0.9 (overl br m, 36H), 3.96 (q, J = 7.2 Hz, 2H), 2.95 (m, 2H), 2.03 (s, 3H), 1.14 (t, J = 7.2 Hz, 3H); IR (KBr pellet) 3437, 2933, 1699, 1652, 1594, 1555, 1458 cm^{-1}; HRMS-ESI (*m/z*): $[M+H]^+$ calcd for $C_{28}H_{50}N_6O_{10}Ga$: 699.2844, obsd 699.2855; t_R (Method B) 15.3 min.

2.2.3.4 Ga-deferoxamine-*n*-propyl carbamate (19)

Compound **19** was prepared from **4** (21.9 mg, 0.034 mmol) using the general procedure in 98% yield (23.7 mg, 0.033). ^{1}H NMR (600 MHz, DMSO-d_6) δ 7.7-7.5 (br m, 2H), 7.04 (m, 1H), 4.0-0.9 (overl br m, 36H), 3.87 (t, J = 6.6 Hz, 2H), 2.95 (m, 2H),

2.03 (s, 3H), 1.54 (m, 2H), 0.87 (t, J = 7.8 Hz, 3H); IR (KBr pellet) 3428, 2935, 1652, 1592, 1456 cm^{-1}; HRMS-ESI (*m/z*): $[M+H]^+$ calcd. for $C_{29}H_{52}N_6O_{10}Ga$: 713.3001, found 713.3006; t_R (Method B) 17.7 min.

2.2.3.5 Ga-deferoxamine-*i*-propyl carbamate (20)

Compound **20** was prepared from **5** (14.5 mg, 0022 mmol) using the general procedure in 95% yield (15.3 mg, 0.021). ^1H NMR (600 MHz, DMSO-d_6) δ 7.7-7.5 (br m, 2H), 6.95 (m, 1H), 4.72 (m, 1H), 4.0-0.9 (overl br m, 36H), 2.94 (m, 2H), 2.03 (s, 3H), 1.14 (d, J = 6.6 Hz, 6H); IR (KBr pellet) 3437, 2933, 1652, 1594, 1458 cm^{-1}; HRMS-ESI (*m/z*): $[M+H]^+$ calcd for $C_{29}H_{52}N_6O_{10}Ga$: 713.3001, obsd 713.3009; t_R (Method B) 16.3 min.

2.2.3.6 Ga-deferoxamine-*n*-butyl carbamate (21)

Compound **21** was prepared from **6** (9.9 mg, 0.015 mmol) using the general procedure in 87% yield (9.5 mg, 0.013 mmol). ^1H NMR (600 MHz, DMSO-d_6) δ 7.7-7.5 (br m, 2H), 7.03 (m, 1H), 4.0-0.9 (overl br m, 36), 3.91 (t, J = 6.6 Hz, 2H), 2.94 (m, 2H), 2.03 (s, 3H), 1.50 (m, 2H), 1.32 (m, 2H), 0.88 (t, J = 7.8 Hz, 3H). IR (KBr pellet) 3436, 2933, 1700, 1653, 1594, 1458 cm^{-1}; HRMS-ESI (*m/z*): $[M+H]^+$ calcd. for $C_{30}H_{54}N_6O_{10}Ga$: 727.3157, obsd 727.3167; t_R (Method B) 17.6 min.

2.2.3.7 Ga-deferoxamine-*i*-butyl carbamate (22)

Compound **22** was prepared from **7** (13.9 mg, 0.021 mmol) using the general procedure in 73% yield (11.1 mg, 0.015 mmol). ^1H NMR (600 MHz, DMSO-d_6) δ 7.7-7.5 (br m, 2H), 7.05 (m, 1H), 4.0-0.9 (overl br m, 36H), 3.70 (d, J = 6.6 Hz, 2H), 2.96 (m,

2H), 2.03 (s, 3H), 1.81 (m, 1H), 0.86 (d, J = 6.6 Hz, 6H). IR (KBr pellet) 3434, 2932, 1700, 1653, 1594, 1459 cm^{-1}; HRMS-ESI (m/z): $[M+H]^+$ calcd for $C_{30}H_{54}N_6O_{10}Ga$: 727.3157, obsd 727.3176; t_R (Method B) 17.5 min.

2.2.3.8 Ga-deferoxamine-Boc (23)

Compound **23** was prepared from **8** (52.7 mg, 0.080 mmol) using the general procedure in 91% yield (53 mg, 0.073 mmol). ^{1}H NMR (600 MHz, DMSO-d_6) δ 7.7-7.5 (br m, 2H), 6.75 (m, 1H), 4.0-0.9 (overl br m, 36H), 2.90 (m, 2H), 2.03 (s, 3H), 1.37 (s, 9H). IR (KBr pellet) 3435, 2933, 1649, 1592, 1454 cm^{-1}; HRMS-ESI (m/z): $[M+H]^+$ calcd for $C_{30}H_{54}N_6O_{10}Ga$: 727.3157, obsd 727.3163; t_R (Method B) 17.2 min.

2.2.3.9 Ga-deferoxamine-*n*-hexyl carbamate (24)

Compound **24** was prepared from **9** (12.5 mg, 0.018 mmol) using the general procedure in 51% yield (6.9 mg, 0.0091 mmol). ^{1}H NMR (600 MHz, DMSO-d_6) δ 7.1-6.7 (br m, 2H), 6.4-6.2 (br m, 1H), 4.5-1.5 (overl br m, 46H), 2.62 (s, 3H), 4.51 (m, 2H), 1.45 (m, 3H). IR (KBr pellet) 3435, 2930, 1653, 1594, 1458 cm^{-1}; HRMS-ESI (m/z): $[M+H]^+$ calcd for $C_{32}H_{58}N_6O_{10}Ga$: 755.3470, obsd 755.3483; t_R (Method B) 19.8 min.

2.2.3.10 Ga-deferoxamine-*n*-hexylamine-Boc carbamate (25)

Compound **25** was prepared from **10** (19.1 mg, 0.024 mmol) using the general procedure in 92% yield (19.2 mg, 0.022 mmol). ^{1}H NMR (600 MHz, DMSO-d_6) δ 7.7-7.5 (br m, 2H), 7.02 (m, 1H), 6.75 (m, 1H), 4.0-0.9 (overl br m, 44H), 3.90 (t, J = 6.6 Hz, 2H), 2.95 (m, 2H), 2.88 (m, 2H), 2.07 (s, 3H), 1.36 (s, 9H). IR (KBr pellet) 3434, 2932,

1699, 1652, 1595 cm^{-1}; HRMS-ESI (*m/z*): $[M+H]^+$ calcd for $C_{37}H_{67}N_7O_{12}Ga$: 870.4104, obsd 870.4120; t_R (Method B) 20.2 min.

2.2.3.11 Ga-deferoxamine-*n*-hexylamine carbamate (26)

Compound **26** was prepared from **11** (11.4 mg, 0.016 mmol) using the general procedure in 44% yield (5.5 mg, 0.0071 mmol). ^{1}H NMR (600 MHz, DMSO-d_6) δ 7.7-7.5 (br m, 2H), 7.04 (m, 1H), 4.0-0.9 (overl br m, 44H), 2.03 (s, 3H), 2.95 (m, 2H), 3.91 (t, J = 6.6 Hz, 2H), 2.62 (t, J = 7.2 Hz, 2H). (Note: NH_2 not obsd). IR (KBr pellet) 3439, 2934, 1652, 1595, 1457 cm^{-1}; HRMS-ESI (*m/z*): $[M+H]^+$ calcd for $C_{32}H_{59}N_7O_{10}Ga$: 770.3579, obsd 770.3593; t_R (Method B) 14.3 min.

2.2.3.12 Ga-deferoxamine-Cbz carbamate (27)

Compound **27** was prepared from **12** (47.3 mg, 0.068 mmol) using the general procedure in 40% yield (20.5 mg, 0.027 mmol). ^{1}H NMR (600 MHz, DMSO-d_6) δ 7.9-7.5 (br m, 2H), 7.4-7.3 (m, 5H), 7.23 (br m, 1H), 5.00 (s, 2H), 4.0-0.9 (overl br m, 36H), 2.99 (m, 2H), 2.02 (s, 3H). IR (KBr pellet) 3422, 2932, 1705, 1652, 1594, 1457 cm^{-1}; HRMS-ESI (*m/z*): $[M+H]^+$ calcd for $C_{33}H_{52}N_6O_{10}Ga$: 761.3000, obsd 761.3013; t_R (Method B) 18.1 min.

2.2.3.13 Ga-deferoxamine-ciprofloxacin (28)

Compound **28** was prepared from **15** (8.0 mg, 0.0083 mmol) using the general procedure reported by Lewis *et al.* in 95% yield (8.2 mg) [25]. ^{1}H NMR (600 MHz, DMSO-d_6) δ 8.67 (s, 1H), 7.93 (m, 1H), 7.81 (m, 1H), 7.58 (m, 1H), 7.7-7.5 (br m, 2H), 4.0-0.9 (overl br m, 55H), 2.03 (s, 3H). IR (KBr pellet) 3439, 2924, 1629, 1473 cm^{-1};

HRMS-ESI (*m/z*): $[M+H]^+$ calcd for $C_{46}H_{66}N_9O_{13}FGa$: 1040.4020, obsd 1040.3971; t_R (Method B) 18.5 min.

2.2.4 Determination of log D

The log *D* values for formulations of ^{67}Ga-**16-28** were determined using the "shake-flask" method [26], (Table 1).

2.2.5 Uptake of ^{67}Ga-DFO and ^{67}Ga-DFO derivatives by *S. aureus, in vitro*.

A scratch from a 20% glycerol preservation culture of *S. aureus* (ATCC25923) was grown for up to 24 h at 37 °C, with shaking, in 45 mL of iron-deficient Tris-Minimal Succinate (TMS) medium [27]. The OD_{600} value of the *S. aureus* culture was determined, then aliquots (normally 3.5 to 4.5 mL) were pelleted by centrifugation at 12,500 × g for 1 min, resuspended once in iron-deficient TMS, pelleted again, then resuspended in 4.5 mL of the appropriate medium (see below) to give an OD_{600} value of 2.0. Media for uptake were prepared by adding ^{67}Ga-DFO, or one of the ^{67}Ga-labelled DFO derivatives, to 5 mL of iron-deficient TMS. For blocking assays, non-radioactive Ga-DFO **16**, with a final concentration of 50 µM, was added to TMS along with the labelled complex. Uptake was initiated by resuspending the bacteria in the media containing the ^{67}Ga derivatives.

During the uptake assays, the *S. aureus* cultures were incubated at 37 °C with shaking at 300 rpm for up to 24 h. Every hour from 0 to 6 h and at 24 h, a 500 µL aliquot was removed and centrifuged at 12,500 × g for 1 min. Ensuring that the bacterial pellet

was not disturbed, 480 µL of supernatant was collected into a 12 × 55 mm Ria plastic test tube (PerkinElmer). The pellet was washed with 500 µL ice-cold PBS and centrifuged at 12,500 × g for 1 min. Again, ensuring that the pellet was not disturbed, 500 µL of supernatant was collected into the same Ria test tube. The pellet was resuspended in 400 µL of 5% (*w/v*) SDS, and allowed to lyse for 30-45 min at room temperature. A 300 µL aliquot of lysed pellet was transferred to a separate Ria test tube for counting. The remaining lysed pellet was frozen at −20 °C for later protein assays. All Ria test tubes were counted for 1 min using Wizard 1470 Automatic Gamma Counter (PerkinElmer) at the end of the assay. Uptake and blocking assays for each ^{67}Ga-labelled compound were performed in duplicate. Uptake was expressed as the percentage (%) of the activity found in the pellet compared to the total activity:

$$\%\ \text{uptake} = \frac{cpm(pellet)}{(cpm(pellet) + cpm(supernatant))} \times 100$$

In order to account for cell growth during the assay, uptake was normalized to the protein concentration, and expressed as % uptake/µg protein. The frozen lysed pellet was thawed at room temperature and protein concentrations were determined following manufacturer's instructions, using Pierce™ BCA Protein Assay Kit, with BSA as a protein standard. The protein concentration in each pellet was determined in triplicate.

2.2.6 Plasma Protein Binding and *In vitro* Stability Studies

In order to determine stability in plasma and protein binding characteristics, a sample of ^{67}Ga-**27** (100 µL, 6.03 MBq) was added to pooled mouse plasma containing Na-Heparin (900 µL) in a 1.5 mL centrifuge tube and incubated at 37 °C. At t = 1, 5, 15,

and 30 min, and 1, 2, 3, and 4 h a sample (100 μL) was taken and added to a microcentrifuge tube containing ice-chilled MeCN (200 μL). The tube was agitated by vortex for 10 sec and the sample separated by centrifugation (20,800 × g, 10 min) to pellet the protein, and the total activity was then measured. The supernatant was removed and the activity in the supernatant and pellet were each measured separately. To assess stability in plasma, the supernatant solutions were analysed by HPLC (Method B), at the indicated time points.

2.2.7 Preparation of *S. aureus*

Staphylococcus aureus (*S. aureus*; ATCC 25293) was obtained from Cedarlane Laboratories Ltd. (Burlington, ON). Several 3 mL overnight cultures were grown in Luria Broth (LB) media (L7658, Sigma-Aldrich Canada, Oakville, ON) at 37°C and 300 rpm. Bacterial cultures were pooled and cells were pelleted at 10,000 × g for 2 min. Cells were washed with sterile PBS (Invitrogen, Mississauga, ON) and centrifuged again at 10,000 × g for 2 min. The pellet was re-suspended and further diluted with sterile PBS to an appropriate concentration for mouse inoculation (2×10^8 colony-forming units (CFU) /mL).

2.2.8 Biodistribution studies in *S. aureus* infected mice.

Animal studies were approved by the Animal Research Ethics Board at McMaster University in accordance with Canadian Council on Animal Care (CCAC) guidelines. BALB/c female mice (5 to 6 weeks old) were purchased from Charles River Laboratories

(Portage, MI) and were maintained under clean, Biohazard Level 2 conditions in an approved animal facility.

Biodistribution studies of ^{67}Ga-**16**, ^{67}Ga-**18**, ^{67}Ga-**26**, and ^{67}Ga-**28** were performed using groups of 12 female BALB/c mice (6 to 7 weeks old) injected with a standard *S. aureus* inoculum into the right thigh muscle (1×10^8 CFU, 50 µL PBS). At 20 h post injection, groups of three infected mice were intravenously injected in the tail vein with 100 µL of PBS containing ~1.33 MBq of ^{67}Ga-**16**, ~1.38 MBq of ^{67}Ga-**18**, ~1.28 MBq of ^{67}Ga-**26** or ~1.07 MBq of ^{67}Ga-**28**. At 1 h post injection, animals were anesthetized with 3% isoflurane and euthanized by cervical dislocation. Blood, kidneys with adrenals, liver with gall bladder, lymph nodes from legs, small intestine (with contents), spleen, left thigh muscle (non-infected), right thigh muscle (infected), and bladder and urine were collected, weighed and counted using a Wizard 1470 Automated Gamma Counter (PerkinElmer, Woodbridge, ON). Tissue distribution data were calculated respect to injected dose (ID) and percentage ID per g organ/tissue (%ID/g). Decay correction was used to normalize organ/tissue radioactivity measurements to the time of dose preparation.

2.3 Results

2.3.1 Synthesis of DFO derivatives

A select number of DFO derivatives have been reported for labelling biomolecules and in particular antibodies [20,25], where the associated chemistry was selected as the initial approach for preparing the library. Unfortunately, it proved to be

non-trivial to prepare simple amide derivatives of DFO beyond the known compounds, as reactions often resulted in impure products having poor solubility that hindered purification. A more convenient and high yielding synthetic method was developed using carbamate-forming reactions that produced a series of novel DFO derivatives in high yield. Reaction of **1** with commercially available alkyl chloroformates gave **2-7**, and **9** in 30-43% yields, where the products could be isolated by preparative HPLC (Scheme 2.1). Alternatively, carbonates could be used as a substitute for the chloroformates and were successfully employed, for example to generate **8**. When the desired chloroformate or carbonate was not commercially available, the corresponding nitrophenylcarbonate was synthesized from bis(4-nitrophenyl) carbonate; an approach that was used successfully to generate **10** and **12**.

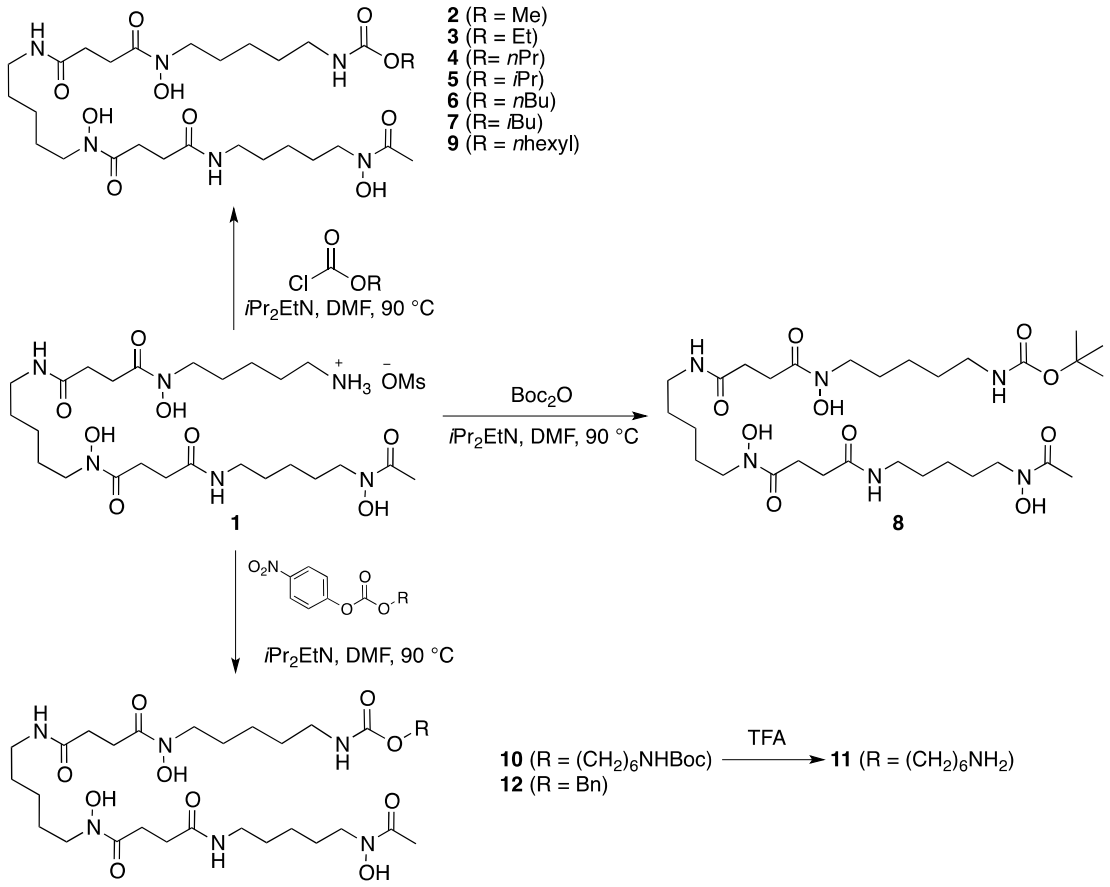

Scheme 2.1 Preparation of deferoxamine carbamates **2-12**.

The preparation of cold Ga complexes to be used as reference standards for the radiolabelling studies was achieved by combining the ligands with excess $Ga(NO_3)_3$. Ga complexed with the DFO ligands was evident in the ^1H NMR spectra, because the N-OH resonances were no longer observed and proton environments close to the metal-chelating hydroxamate groups, including the alkyl backbone of the ligand, appeared significantly broadened (Supplementary Information). Raymond and colleagues reported that there are eight distinct geometric isomers for the metal complexes; however, only

two isomers are present in solution [21]. Well-resolved signals were observed for the carbamate substituents distant from the metal coordinated hydroxamate groups. HPLC of **17-27** revealed single peaks and the HRMS data was consistent with the values expected for the proposed products.

2.3.2 Radiosynthesis

The labelling of the DFO derivatives proceeded at room temperature using a method adapted from Petrik *et al.* (Scheme 2.2) [15].

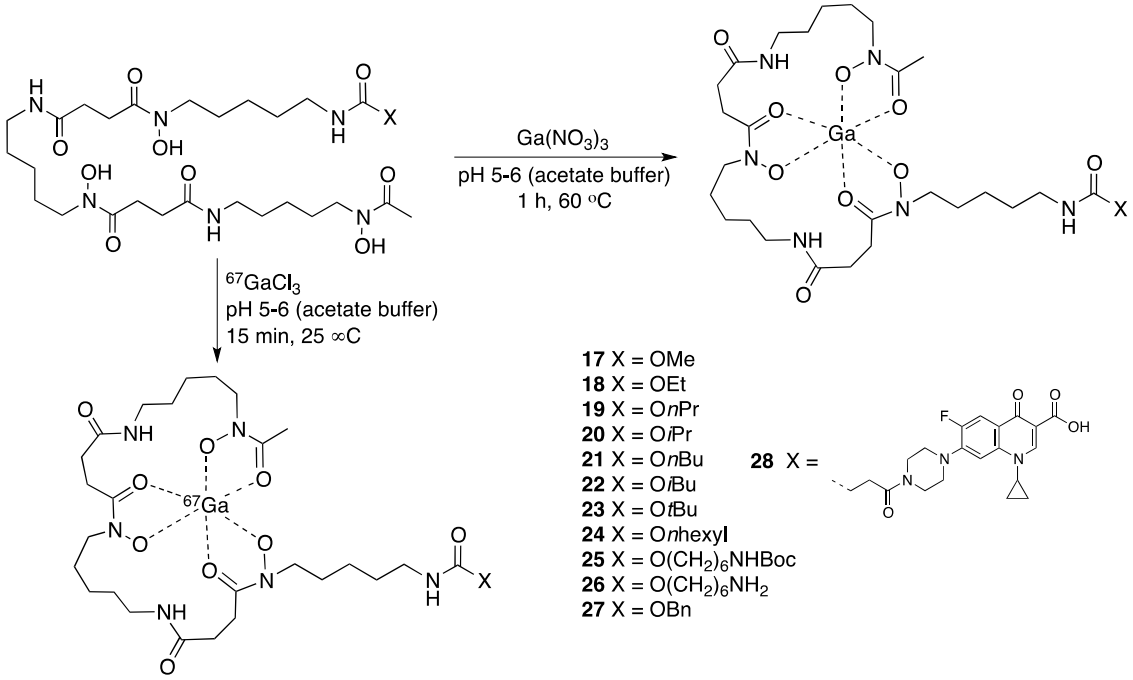

Scheme 2.2 Preparation of Ga and ^{67}Ga complexes **17-28**.

Radiochemical yields were generally greater than 90% with radiochemical purities > 95%. γ-HPLC traces showed a single peak in all cases and the retention times for the products matched those for the UV-HPLC chromatograms of the Ga reference

standards (Figure 2.1). Chromatograms for all compounds can be found in the Supplementary Information.

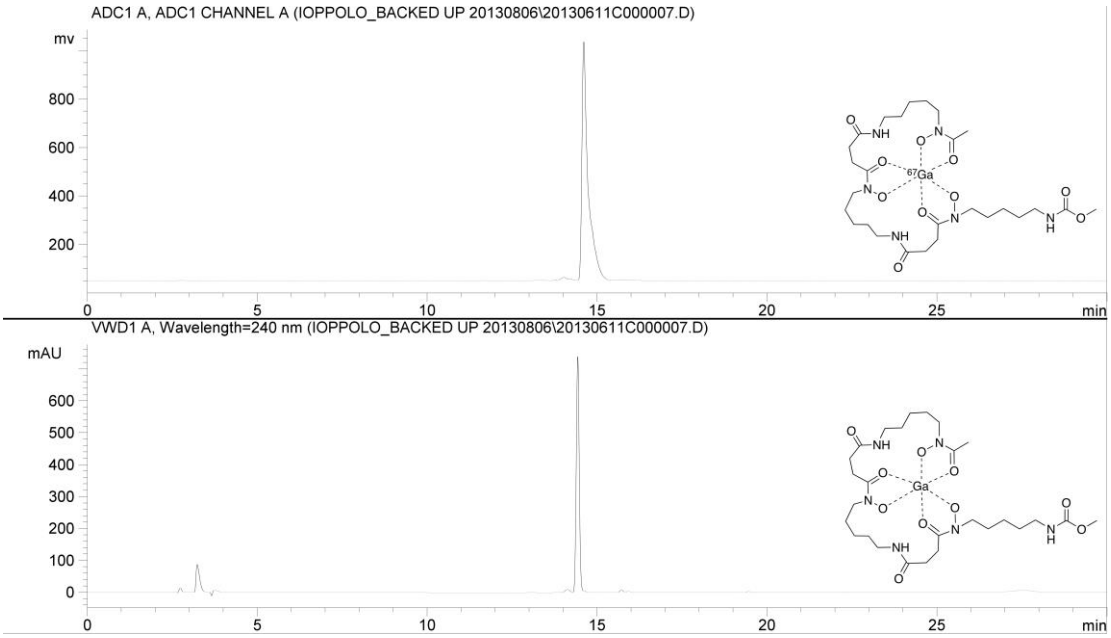

Figure 2.1 Radio-HPLC (top) and UV-HPLC (λ = 240 nm) chromatograms of [^{67}Ga]-**17** spiked with the non-radioactive reference standard (HPLC Method B). Chromatograms for all reported compounds can be found in the Supplementary Information.

2.3.3 Log *D*, stability, and plasma binding

Lipophilicity of the various DFO derivatives was measured by determination of the 1-octantol:PBS partition coefficient (pH 7.4) [26]. It was found that log *D* values generally correlated with the length of the carbon chain attached to the chelate (Figure 2.2). For instance, the most polar compound was the Ga-DFO complex **16** (log *D* = -3.04

± 0.18), followed by **26** that contained an alkyl chain with a terminal amine group (log *D* = -2.05 ± 0.02). Compounds **24** and **25**, which contained hexyl spacers were the most lipophilic (log *D* = 1.17 ± 0.05 and log *D* = 1.08 ± 0.03, respectively).

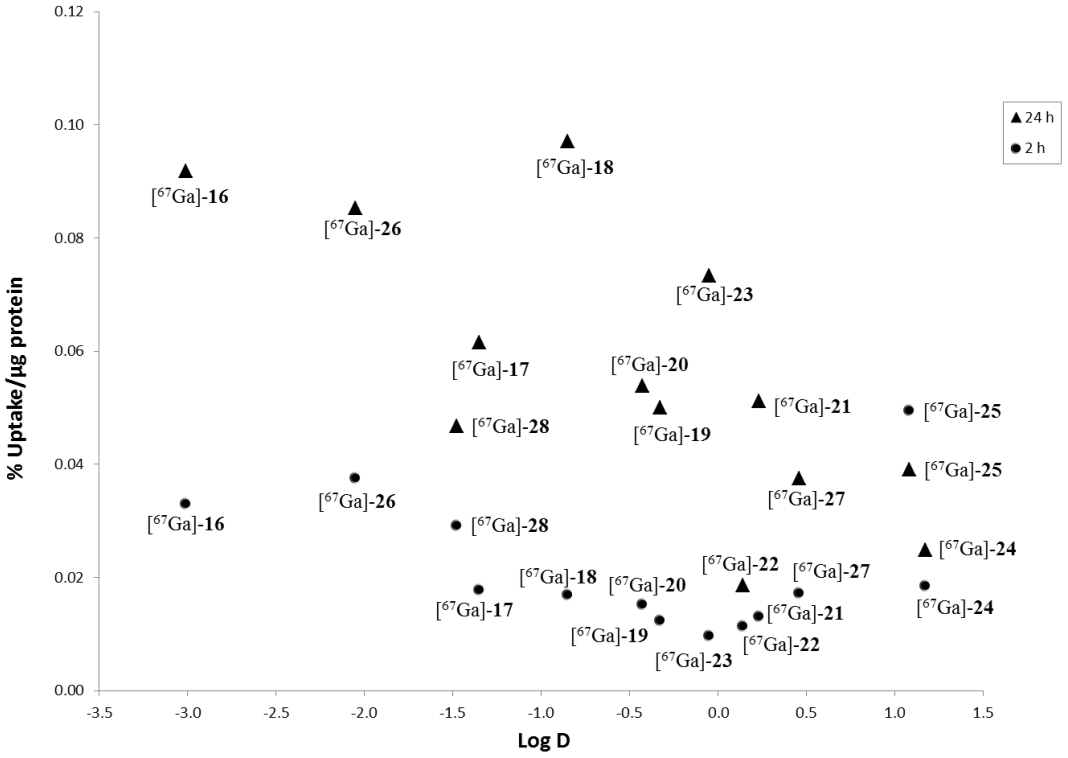

Figure 2.2 Uptake by *S. aureus* compared to log *D* for [^{67}Ga]-**16**-**28**. Plot of the percentage of initial radioactivity bound per µg protein versus log *D* at 2 h (circle) and 24 h (triangle).

The stability of the ^{67}Ga-labelled complexes in PBS at room temperature, were evaluated by analytical HPLC over 24 h. No change in the γ-traces were observed over this time period. The stability and protein binding in plasma was assessed using ^{67}Ga-**27**

as a representative compound (Figure 2.3). The product showed low binding to plasma proteins after 3 h (3.4% unbound at 3 h). Following the same protocol, ^{67}Ga-**16** exhibited similar plasma binding (4.6% at 3 h). The stability of ^{67}Ga-**27** in plasma at 3 h was > 97% and was similar to that observed for **16**.

A. Plasma Protein Binding B. Stability in Plasma

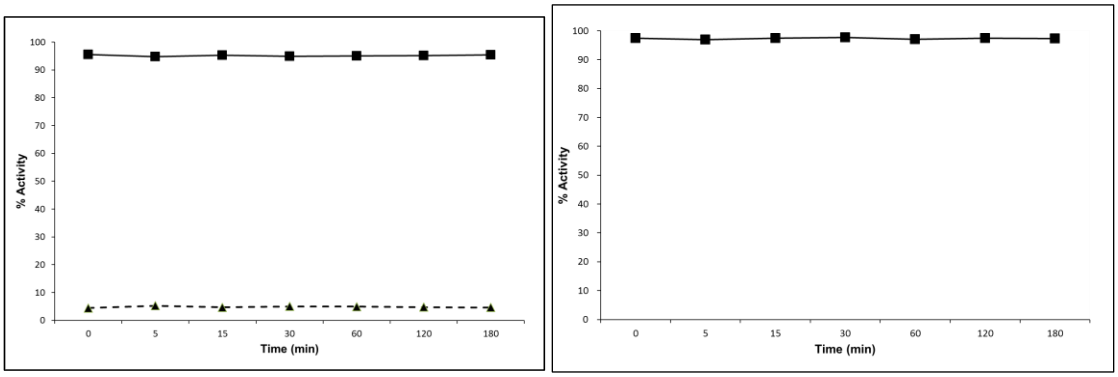

Figure 2.3 Plasma protein binding (A) and stability in plasma (B) for ^{67}Ga-**27**. In A, radioactivity protein bound, in the precipitate (dashed line) or soluble in supernatant (solid line) are expressed as a percentage of the total radioactivity. In B, radio-HPLC (Method B) was performed on supernatants to determine % of radioactivity represented by intact ^{67}Ga-**27**.

2.3.4 *S. aureus* uptake studies

S. aureus was used to evaluate the impact of derivatization on the uptake of the metal complexes in bacteria. *S. aureus* is frequently listed as antibiotic resistant and is responsible for approximately two thirds of all healthcare associated infections [28]. The uptake of ^{67}Ga-**16** by the bacteria served as the point of reference for the radiolabelled

DFO derivatives compounds, and was performed at both 4 °C and 37 °C. As expected, significantly greater and gradually increasing uptake occurred over 6 h at 37 °C but not at 4 °C (Supplementary Information). This suggests that ^{67}Ga-**16** is taken up by *S. aureu*s via active transport. Specific versus non-specific uptake was tested through a competitive blocking experiment using the cold Ga-DFO complex.

The control ^{67}Ga-**16** showed a near-linear uptake for the first 6 h, rising to a maximum of 0.14% /μg protein at 6 h (Supplementary Information). The uptake at 24 h revealed that in the intervening period, there was a marked decrease in apparent uptake with 0.09% /μg protein remaining at the time of analysis. This may be due to the efflux of ^{67}Ga-**16**; however, further experiments are necessary to rule out cell death and lysis. The uptake profile of the new ^{67}Ga-DFO complexes was, apart from a few cases, similar to ^{67}Ga-**16**, although the kinetics were frequently slower (Figure 2.2). Unlike the control, uptake over this time appeared to follow a monotonic linear trend between incubation time and uptake with no major efflux between 6 h and 24 h with the exception of small levels observed for ^{67}Ga-**18** after 6 h. The uptake of ^{67}Ga-**18**, ^{67}Ga-**23**, and ^{67}Ga-**26** were on par with ^{67}Ga-DFO at 24 h, despite their lower uptake at earlier time points.

In general, slower uptake was observed for the more lipophilic complexes (Fig. 3). This is evident when comparing ^{67}Ga-**17** (log $D_{7.4}$ −1.35 ± 0.01) with ^{67}Ga-**23** (log D −0.05 ± 0.05). After 6 h, roughly twice as much ^{67}Ga-**17** was taken up into the bacteria as ^{67}Ga-**23**. The *n*-hexyl-containing ^{67}Ga-**24** (log D 1.17 ± 0.05) also had poor uptake kinetics. ^{67}Ga-**25**, also highly lipophilic (log D 1.08 ± 0.03), was the exception in that it showed decreasing uptake over time despite initial high binding. A plot of percent uptake

per microgram of protein at 2 and 24 h versus log *D* for all compounds generally shows greater uptake for more hydrophilic compounds and suggests that compounds ^{67}Ga-**18** and ^{67}Ga-**26** appeared to be the most promising (Figure 2.2).

2.3.5 Biodistribution studies

Biodistribution studies of ^{67}Ga-**16**, ^{67}Ga-**18**, and ^{67}Ga-**26** were performed using BALB/c mice injected with *S. aureus* in the right thigh, and vehicle in the left thigh as a control. ^{67}Ga-**18** showed the highest infected thigh to non-infected thigh ratio of 11, while the ratio for [^{67}Ga]-**16** was 6.3:1 (Figure 2.4). The infected thigh to blood ratio of 5.4:1 for [^{67}Ga]-**18** was comparable to [^{67}Ga]-**16**.

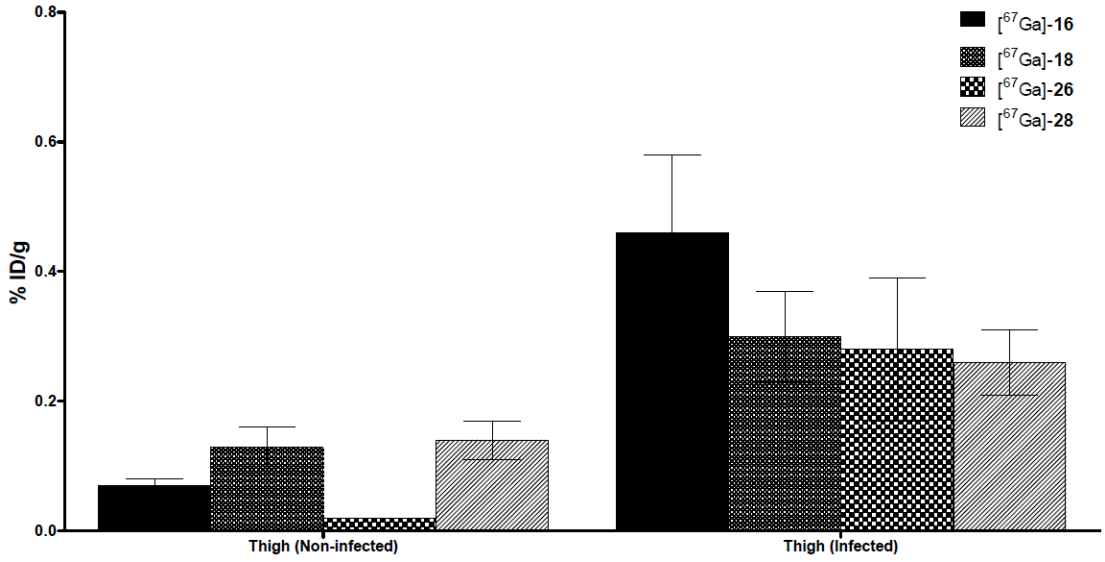

Figure 2.4 Ratio of the percent injected dose per gram (ID%/g) in mouse non-infected versus *S. aureus* infected thigh muscle. Mice were injected with [^{67}Ga]-**16**, [^{67}Ga]-**18**, [^{67}Ga]-**26** and [^{67}Ga]-**28**. Uptake was determined at 20 h post *S. aureus* infection and 1 h after administration of the tracer.

The main route of clearance for the derivatives studied was through the bladder and urine. Furthermore, considerable uptake in the small intestine was observed for all derivatives in comparison to [^{67}Ga]-**16** (Figure 2.5).

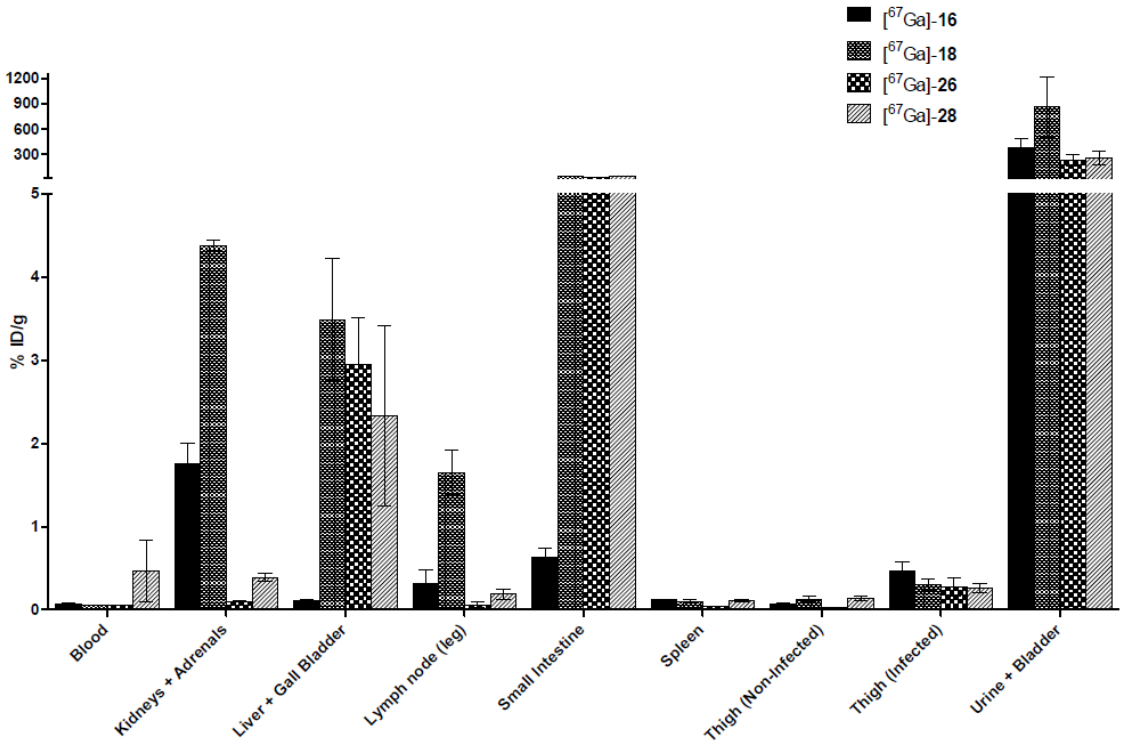

Figure 2.5 Biodistribution (%ID /g) data for [^{67}Ga]-**16**, [^{67}Ga]-**18**, [^{67}Ga]-**26** and [^{67}Ga]-**28** in mice with single thigh infection of *S. aureus.* Data shown are mean ± SEM (n=3). Complete biodistribution data can be found in the Supplementary Information.

The impact of adding a targeting agent was also assessed where DFO was linked to the antibiotic ciprofloxacin (Scheme 2.3) and the biodistribution of the [^{67}Ga] labelled product **28** assessed. This particular vector was selected as a comparator since

radiolabelled ciprofloxacin showed early promise as radiopharmaceuticals for imaging infection [29]. [^{67}Ga]-**28** showed high uptake in the intestine and had a poor infected thigh to non-infected thigh ratio of 1.84:1 which was less than that observed for [^{67}Ga]-DFO alone.

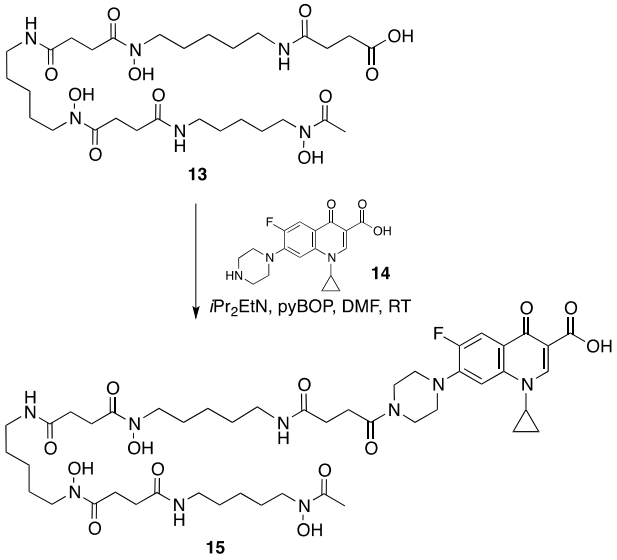

Scheme 2.3 Preparation of the DFO-ciprofloxacin conjugate **15**.

2.4 Discussion

There are a number of limitations with current radiopharmaceuticals for imaging infection, including poor ability to distinguish infection from tumours, inflammation and infection (FDG probes), and slow target-to-non-target binding, requiring long clearance times ([^{67}Ga]-citrate). An alternative approach is to target biochemical systems that are unique to bacteria in order to improve specificity. For instance, radio-gallium analogues of iron siderophores have the potential to selectively image infection by targeting the

bacterial iron sequestering mechanism. Unfortunately, Ga derivatives of DFO, one of the most readily available siderophores, are excreted too rapidly to be a useful infection probe.

A library of DFO derivatives was prepared and radiolabelled to assess the impact of substitution on the uptake and retention in *S. aureus*. If derivatization has minimal impact on uptake, then different substituents can be used to prolong circulation and change the route and/or kinetics of clearance, as means of increasing the likelihood of interaction and uptake of the tracer at the site of infection. To this end DFO derivatives with a range of different substituents were prepared by reaction of **1** with chloroformates, carbonates or nitrophenylformates (Scheme 2.1). The synthetic route using the carbonates were generally high yielding (74-93%) and the products could be purified by recrystallization unlike for the chloroformates (30-43%), where HPLC purification was necessary. This is most likely due to a competing reaction between chloroformate and the free N-OH groups, resulting in a number of side products. For example, when an excess of *i*-butylchloroformate (5 equiv.) was used to prepare **7**, the mono, di, tri and tetra-substituted products were formed, as evident by ESI-MS (*m/z* 661.4, 761.4, 861.5 and 961.5, respectively). Reaction with (4-nitrophenyl)carbonates was a highly effective alternative that showed no evidence of reactions with N-hydroxy groups. Using this approach, *N*-carbamate-derivatized DFO compounds could be readily prepared representing a convenient new strategy for functionalizing the siderophore.

Following preparation of the desired DFO ligands, complexation with excess $Ga(NO_3)_3$ yielded the desired metal complexes for use as HPLC standards. In general, the

radiosyntheses of [^{67}Ga]-**17**-**28** was successful, and the products showed high radiochemical purity (Scheme 2.2). The radiolabelled compounds showed no signs of degradation for up to one week at room temperature when formulated in PBS.

The log $D_{7.4}$ values for this library of compounds ranged from the most lipophilic derivative ([^{67}Ga]-**24**, 1.17 ± 0.05) to least lipophilic derivative ([^{67}Ga]-**26**, −2.05 ± 0.02) (Table 2.1). The measured log $D_{7.4}$ for the control [^{67}Ga]-**16** was −3.04 ± 0.18 which is similar to a previously reported value (−3.56 ± 0.17) [15]. The choice of these simple alkyl groups afforded compounds with a range of steric influence and log $D_{7.4}$ values, from which to start to investigate the effect of substitution on bacterial uptake.

Table 2.1 Experimentally determined, 1-octanol:PBS (pH = 7.4) partition coefficients (log *D*) for compounds **16**-**28**.

Compound	log *D*
[^{67}Ga]-**16**	−3.04 ± 0.18
[^{67}Ga]-**17**	−1.35 ± 0.01
[^{67}Ga]-**18**	−0.85 ± 0.01
[^{67}Ga]-**19**	−0.33 ± 0.01
[^{67}Ga]-**20**	−0.43 ± 0.01
[^{67}Ga]-**21**	0.23 ± 0.01
[^{67}Ga]-**22**	0.14 ± 0.01
[^{67}Ga]-**23**	−0.05 ± 0.05

[^{67}Ga]-**24**	1.17 ± 0.05
[^{67}Ga]-**25**	1.08 ± 0.03
[^{67}Ga]-**26**	−2.05 ± 0.02
[^{67}Ga]-**27**	0.46 ± 0.07
[^{67}Ga]-**28**	−1.48 ± 0.01

Following confirmation of active uptake of [^{67}Ga]-**16** *in vitro* with *S. aureus*, the uptake profile of each of the complexes [^{67}Ga]-**17-28** was studied (Figure 2.2). As a general trend, the rate of uptake decreased as the lipophilicity of the complex increased. Interestingly, the early uptake of [^{67}Ga]-**26** was rapid with higher uptake into *S. aureus* than the DFO complex at early time points (1 h and 2 h). The compound demonstrated local minima in the uptake profile at 5 h, which was observed in all repeat assays and is mostly likely due to a secondary interaction with the bacteria, though the exact mechanism remains to be elucidated. It was also noted that the terminal amine in [^{67}Ga]-**26** as well as in the control [^{67}Ga]-**16** seemed to enhance uptake, which may be due to interaction of the positively charged amine with the anionic phospholipids and related amphiphilic structures that reside within the bacterial envelope [30-32]. For [^{67}Ga]-**28**, favourable early uptake may be attributed to recognition of the presence of the ciprofloxacin, where radiolabelled analogues have been investigated previously as infection imaging probes [29,33,34].

A preliminary biodistribution was performed in BALB/c mice bearing a *S. aureus* infection in the thigh using the method reported for evaluating biodistribution of [^{67}Ga]-citrate [2,35,36]. Mice received 1×10^8 CFU in the muscle and the lead tracers [^{67}Ga]-**18** and [^{67}Ga]-**26** and [^{67}Ga]-**16** as the control were administered 20 hours post-inoculation and animals sacrificed at one hour. It should be noted that prior to evaluating the DFO derivatives, the model was validated by performing a [^{67}Ga]-citrate biodistribution where the data obtained was similar to that reported in the literature. Following necropsy, the bacteria were cultured and were shown to grow, indicating active infections.

The biodistribution of ^{67}Ga-DFO was consistent with the literature and showed the high uptake in the bladder with minimal uptake in all other organs with the exception of the kidney (1.75 %ID/g ± 0.75%). Uptake in the infected (right) thigh was 0.46 %ID/g ± 0.12 which was greater than the control (left) thigh (0.07 %ID/g ± 0.01). [^{67}Ga]-**18** by comparison also showed high bladder uptake; however, the small intestine showed appreciable uptake (30.04 %ID/g ± 2.45) that was significantly higher than [^{67}Ga]-**16** (0.63 %ID/g ± 0.11). The increased lipophilicity was also observed by the increased liver uptake (2.95 %ID/g ± 0.57). Higher uptake in the intestines was noted for the ciprofloxacin derivative (46.27 %ID/g ± 2.69). All compounds exhibited rapid blood clearance.

With respect to uptake ratios between the infected (RT) and non-infected (LT) thighs, [^{67}Ga]-**22** showed the highest at 11:1 whereas [^{67}Ga]-DFO **16** was 6.3:1. [^{67}Ga]-**18** showed similar RT:blood ratio (5.4:1). Interestingly, using a direct targeting construct

was not beneficial where [^{67}Ga]-**28** the ciprofloxacin derivative, showed the poorest contrast between the infected and non-infected thighs.

2.5 Conclusion

We have shown that it is possible to functionalize DFO and to retain active uptake in *S. aureus* in vitro. While good selectivity between the infected and non-infected thighs were seen for select compounds relative to [^{67}Ga]-DFO, the total uptake and residual binding in the GI tract will hinder the use of the current derivatives as infection imaging agent. It is however possible to expand the library using the synthetic strategy developed here to continue to refine the pharmacokinetics. In addition, given the recent work using non-radioactive Ga-DFO derivatives as therapeutic agents [16], the reported compounds may have utility as adjuvants to standard antibiotics.

References

[1] Bleeker-Rovers CP, Vos FJ, van der Graaf WTA, Oyen WJG. Nuclear medicine imaging of infection in cancer patients (with emphasis on FDG-PET). Oncologist 2011;16:980–91.

[2] Bettegowda C, Foss CA, Cheong I, Wang Y, Diaz L, Agrawal N, Fox J, Dick J, Dang LH, Zhou S. Imaging bacterial infections with radiolabeled 1-(2'-deoxy-2'-fluoro-beta-D-arabinofuranosyl)-5-iodouracil. Proc Natl Acad Sci USA. 2005;102:1145–50.

[3] Rennen HJJM, Boerman OC, Oyen WJG, Corstens FHM. Imaging infection/inflammation in the new millennium. Eur J Nucl Med 2001; 28:241–52.

[4] Kumar V. Radiolabeled white blood cells and direct targeting of micro-organisms for infection imaging. QJ Nucl Med Mol Imaging 2005;49:325–38.

[5] Love C, Tomas MB, Tronco GG, Palestro CJ. FDG PET of infection and inflammation Radiographics 2005;25:1357–68.

[6] Sugawara Y, Gutowski TD, Fisher SJ, Brown RS, Wahl RL. Uptake of positron emission tomography tracers in experimental bacterial infections: a comparative biodistribution study of radiolabeled FDG, thymidine, L-methionine, 67Ga-citrate, and 125I-HAS. Eur J Nucl Med 1999;26:333–41.

[7] Weinstein EA, Ordonez AA, DeMarco VP, Murawski AM, Pokkali S, MacDonald EM, Klunk M, Mease RC, Pomper MG, Jain SK. Imaging enterobacteriaceae infection in vivo with 18F-fluorodeoxysorbitol positron emission tomography Sci Transl Med 2014;6:259ra146.

[8] Van Oosten M, Schäfer T, Gazendam JaC, Ohlsen K, Tsompanidou E, de Goffau MC, Harmsen HJM, Crane LM, Lim E, Francis KP, Cheung L, Olive M, Ntziachristos V, van Dijl JM, van Dam GM. Real-time in vivo imaging of invasive- and biomaterial-associated bacterial infections using fluorescently labelled vancomycin Nat Commun 2013;4:2584.

[9] Ning X, Lee S, Wang Z, Kim D, Stubblefield B, Gilbert E, Murthy N. Maltodextrin-based imaging probes detect bacteria in vivo with high sensitivity and specificity. Nat Mater 2011;10:602–7.

[10] Ning X, Seo W, Lee S, Takemiya K, Rafi M, Feng X, Weiss D, Wang X, Williams L, Camp VM. PET imaging of bacterial infections with fluorine-18-labeled maltohexaose Angew Chem Int Ed 2014;126:14320–25.

[11] Braun V. Iron uptake mechanisms and their regulation in pathogenic bacteria. Int J Med Microbiol 2001;291:67–79.

[12] Merkx M, Averill BA. Probing the role of the trivalent metal in phosphate ester hydrolysis: Preparation and characterization of purple acid phosphatases containing (AlZnII)-Zn-III and (InZnII)-Zn-III active sites, including the first example of an active aluminum enzyme. J Am Chem Soc 1999;121:6683–9.

[13] Zhai C, Summer D, Rangger C, Haas H, Haubner R, Decristoforo C. Fusarinine C, a novel siderophore-based bifunctional chelator for radiolabeling with Gallium-68. J Labelled Compd Radiopharm 2015;58:209–14.

[14] Emery T, Hoffer PB. Siderophore-mediated mechanism of gallium uptake demonstrated in the microorganism Ustilago sphaerogena. J Nucl Med 1980;21:935–9.

[15] Petrik, M.; Haas, H.; Schrettl, M.; Helbok, A.; Blatzer, M.; Decristoforo, C. In vitro and in vivo evaluation of selected 68Ga-siderophores for infection imaging. Nucl Med Biol 2012;39:361–9.

[16] Banin E, Lozinski A, Brady KM, Berenshtein E, Butterfield PW, Moshe M, Chevion M, Greenberg EP, Banin E. The potential of desferrioxamine-gallium as an anti-Pseudomonas therapeutic agent. Proc Natl Acad Sci USA 2008;105:16761–6.

[17] Herscheid JDM, Hoekstra A, Vos CM. N-Succinyldesferrioxamine B: a potential radiopharmaceutical for assessing renal function. Eur J Nucl Med 1984;9:508–10.

[18] Hersheid JDM, Knops G, Hoekstra M. The biodistribution of 67Ga-labelled N-hydroxyamino acid derivatives in tumour-bearing rats. Nucl Med Commun 1986;7:53–8.

[19] Patil KM, Naik RJ, Fernandes M, Ganguli M, Kumar VA. Highly efficient (R-X-R)-type carbamates as molecular transporters for cellular delivery. J Am Chem Soc 2012;134:7196–9.

[20] Verel I, Visser,, GWM, Boellaard R, Stigter-van Walsum M, Snow GB, van Dongen G. A. 89Zr immuno-PET: comprehensive procedures for the production of 89Zr-labeled monoclonal antibodies. J. Nucl. Med. 2003;44:1271–81.

[21] Borgias B, Hugi AD, Raymond KN. Isomerization and solution structures of desferrioxamine-B complexes of Al-3+ and Ga-3+1. Inorg Chem 1989;28:3538–45.

[22] Bergeron R J, McManis JS, Phanstiel OIV, Vinson JRT. A versatile synthesis of deferrioxamine-B. J Org Chem 1995;60:109–14.

[23] Prelog V, Walser A. Über die synthese der ferrioxamine B und D1. Helv Chim Acta 1962;45:631–7.

[24] Ji C, Miller MJ. Chemical syntheses and in vitro antibacterial activity of two desferrioxamine B-ciprofloxacin conjugates with potential esterase and phosphatase triggered drug release linkers. Bioorg Med Chem 2012;20:3828–36.

[25] Zeglis, B. M.; Mohindra, P.; Weissmann, G. I.; Divilov, V.; Hilderbrand, S. A.; Weissleder, R.; Lewis, J. S. *Bioconjug. Chem.* **2011**, *22*, 2048–2059.

[26] Wilson AA, Jin L, Garcia A, DaSilva JN, Houle S. An admonition when measuring the lipophilicity of radiotracers using counting techniques. Appl Radiat Isot 2001;54;203–8.

[27] Sebulsky MT, Speziali CD, Shilton BH, Edgell DR, Heinrichs DE. FhuD1, a ferric hydroxamate-binding lipoprotein in Staphylococcus aureus: a case of gene duplication and lateral transfer. J Biol Chem 2004;279:53152–9.

[28] Edelsberg J, Taneja C, Zervos M, Haque N, Moore C, Reyes K, Spalding J, Jiang J, Oster G. Trends in US hospital admissions for skin and soft tissue infections. Emerg Infect Dis 2009;15:1516-8.

[29] Britton KE, Wareham DW, Das SS, Solanki KK, Amaral H, Bhatnagar A, Katamihardja AHS, Malamitsi J, Moustafa HM, Soroa VE. Imaging bacterial infection with (99m)Tc-ciprofloxacin (Infecton). J Clin Pathol 2002;55:817–23.

[30] DiVittorio KM, Leevy WM, O'Neil EJ, Johnson JR, Vakulenko S, Morris JD, Rosek KD, Serazin N, Hilkert S, Hurley S. Zinc(II) coordination complexes as membrane-active fluorescent probes and antibiotics. ChemBioChem 2008;9:286–93.

[31] Ganesh V, Bodewits K, Bartholdson SJ, Natale D, Campopiano DJ, Mareque-Rivas JC. Effective binding and sensing of lipopolysaccharide: combining complementary pattern recognition receptors. Angew Chemie Int Ed 2009;48:356–60.

[32] White AG, Fu N, Leevy WM, Lee JJ, Blasco MA, Smith BD. Optical imaging of bacterial infection in living mice using deep-red fluorescent squaraine rotaxane probes. Bioconjug Chem 2010;21:1297–1304.

[33] Sarda L, Crémieux AC, Lebellec Y, Meulemans A, Lebtahi R, Hayem G, Génin R, Delahaye N, Huten D, Le Guludec D. Inability of 99mTc-ciprofloxacin scintigraphy to discriminate between septic and sterile osteoarticular diseases. J Nuc Med 2003;44:920–6.

[34] Sonmezoglu K, Sonmezoglu M, Halac M, Akgün I, Türkmen C, Önsel C, Kanmaz B, Solanki K, Britton KE, Uslu I. Usefulness of 99mTc-ciprofloxacin (infecton) scan in diagnosis of chronic orthopedic infections: comparative study with 99mTc-HMPAO leukocyte scintigraphy. J Nucl Med 2001;42:567–74.

[35] Ferro-Flores G, de Murphy CA, Pedraza-López M, Meléndez-Alafort L, Zhang YM, Rusckowski M, Hnatowich DJ. In vitro and in vivo assessment of 99mTc-UBI specificity for bacteria. Nucl Med Biol 2003;30:597–603.

[36] Tsopelas C, Penglis S, Bartholomeusz FDL. Comparison of 99mTc-alafosfalin and 67Ga-citrate in a mouse model of bacterial infection. Nucl Med Rev 2002;5:93–7.

Chapter 3

3 Development of ^{67}GaDFO based Molecular Imaging Agents for Bacterial Infections

With the low uptake seen with DFO derivatives and direct targeting, an alternative approach using pretargeting strategy was explored. The approach uses vancomycin as a targeting vector and biorthogonal chemistry to link the antibiotic to a radiolabeled ligand. The approach uses a rapid and highly selective coupling reaction between *trans*-cyclooctenes (TCO) and tetrazines.

3.1 Bioorthogonal Chemistry

3.1.1 Pretargeting Approaches for Molecular Imaging

The success of molecular imaging probes is highly dependent on the pharmacokinetic properties of the construct. Ideal targeting vectors must have high specificity and binding affinity towards the target of interest, have low non-specific binding elsewhere, be metabolically stable, and have low immunogenicity.[1–3] However, designing and developing desirable molecular imaging probes to meet all of these properties remains a challenge. An alternative approach to directly labeling a targeting vector has emerged which involves pretargeting prior to administration of the actual imaging agent.

Pretargeting is a two-step approach that involves the administration of the targeting vector followed by intravenous administration of an imaging agent that binds to the targeting vector *in vivo*. It is important to allow sufficient time following the administration of the targeting vector for the compound to clear non-target tissues prior to the administration of the second agent.[2] Bioorthogonality, which is required for the two components to selectively co-locate, is defined as a chemical reaction that is biocompatible, nontoxic, and selective towards the participating functional groups while inert against all other species present in a biological system.[4] While many bioorthogonal reactions exist, one showing great promise is the inverse electron-demand Diels-Alder cycloaddition reactions between tetrazines and *trans*-cyclooctene derivatives.

3.1.2 Inverse Electron-Demand Diels-Alder Cycloaddition Reactions

In 1990, Thalhammer *et al.* studied the kinetics of the reaction of electron deficient tetrazine with various dienophiles and reported that the rate between tetrazines and *trans*-cyclooctene (Scheme 3.1) to be the fastest.[5] However, the tetrazine derivatives were reactive towards water. In 2008, Blackman *et al.* demonstrated the bioorthogonality of 3,6-diaryl-*s*-tetrazine and *trans*-cyclooctene with very fast kinetics ($k_2 > 10^3$ M^{-1} s^{-1}), where k_2 is the second order rate constant.[6] This ground-breaking publication led to extensive research in using *s*-tetrazine and *trans*-cyclooctene derivatives as bioorthogonal partners to aid in the development of imaging and therapeutic agents.

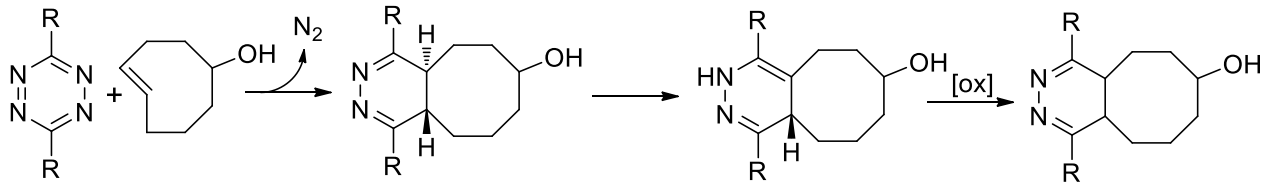

Scheme 3.1 Inverse electron-demand Diels-Alder cycloaddition between an *s*-tetrazine (R=CO_2Me or CF_3) and (*E*)-cyclooct-4-enol.[7]

Radiolabeled tetrazine derivatives have been used in an increasing number of pretargeting applications with a wide range of different isotopes including ^{64}Cu,[8] ^{111}In,[9] ^{177}Lu,[10] ^{68}Ga,[11] and ^{18}F.[12] In one example, Rossin and coworkers reported a pretargeted approach using the Tz-TCO reaction for imaging tumours *in vivo* which showed images of exceptional quality.[10] The availability of radiolabeled tetrazines, when combined with the prior success of TCO-functionalized vancomycin based optical and magnetic imaging of infections suggests there is an opportunity to use pretargeting for imaging infection.

Vancomycin is an antibiotic (Figure 3.1) isolated from *Streptomyces orientalis* that has activity against Gram-positive bacteria.[13] It binds to the acyl-D-alanyl-D-alanine amino acid moiety of bacterial cell walls and prevents the cross-linking of peptidoglycan.[14] Recent studies have demonstrated the specificity of vancomycin-TCO towards Gram-positive bacteria,[15] and the binding of vancomycin to intracellular bacteria within macrophages due to its permeability towards mammalian cell membranes.[16]

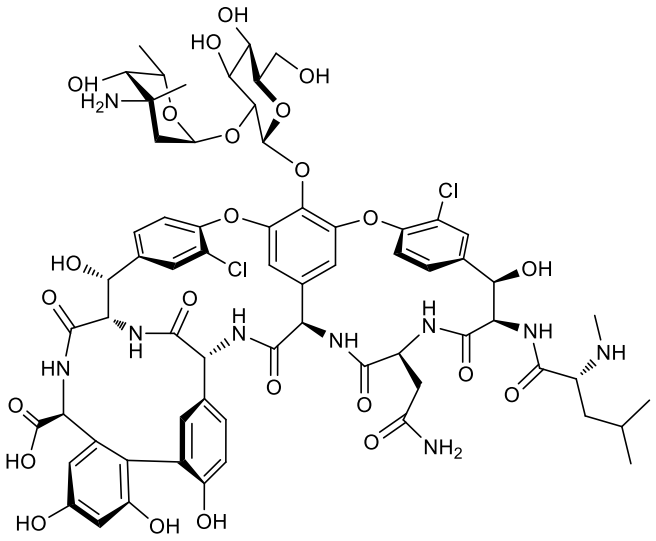

Figure 3.1 Structure of vancomycin

3.1.3 Vancomycin

Radiolabeled vancomycin using various isotopes have been reported in literature and studied both *in vivo* and *vitro*.[13,17,18] However, the one reported *in vivo* study had a number of shortcomings.[17] Most notably, the biodistribution data was missing critical organs including the relative uptake in infected versus non-infected thighs, and the levels of activity in the blood and intestines. Furthermore, the latest time point studied was only 60 minutes. For ^{99m}Tc-vancomycin-chelator conjugates, the reported *in vitro* studies also had some shortcomings.[18] The binding assay results were only reported for the 2 hour time point and the data did not indicate whether or not cell growth was a critical factor.

Vancomycin is primarily eliminated through renal clearance in patients with normal renal function.[19] Recently, studies have shown that the clearance of vancomycin is decreased in patients with impaired liver function, demonstrating the role of liver in the elimination of vancomycin.[20] This explains the measurable uptake of ^{99m}Tc-vancomycin

by the liver reported by Roohi *et al*.[17] A pretargeted strategy would take advantage of bacteria-specific targeting properties of vancomycin and fast clearance of small imaging agents from GI tract and other organs.

Weissleder *et al.* showed that vancomycin-*trans*-cyclooctene (vancomycin-TCO) could be used to ligate tetrazine functionalized magnetofluorescent nanoparticles to bacterial infections *in vitro*. Their results demonstrated the dose-dependent binding of vancomycin-TCO to Gram-positive bacteria. Due to the limitations of optical and magnetic imaging techniques, pretargeting strategies using a ^{67}GaDFO tetrazine (^{67}GaDFO-Tz) and vancomycin-TCO was evaluated as a new approach for imaging *S. aureus in vitro* and *in vivo* (Scheme 3.2). If successful, this approach can be readily expanded since a wide variety of different antibiotics, which have high affinity and specificity towards bacteria, can be used as targeting vectors for imaging infections.[21]

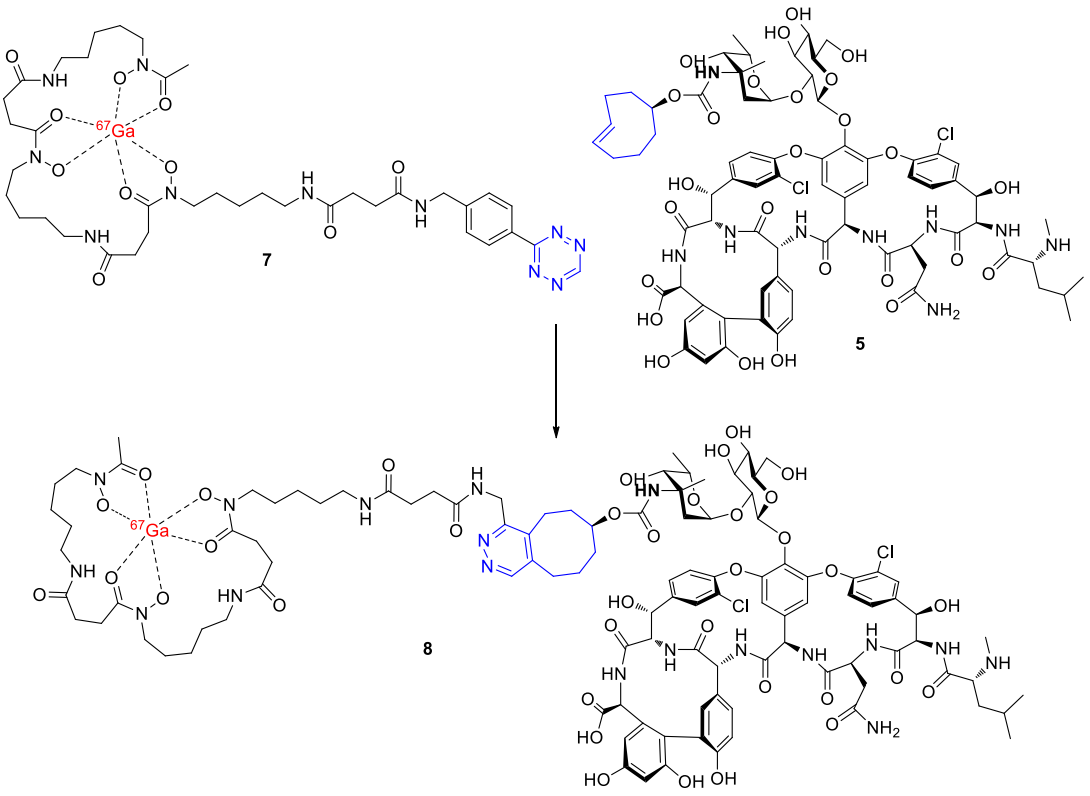

Scheme 3.2 Preparation of ^{67}GaDFO-Tz-vancomycin-TCO conjugate **8** complex.

3.2 Methods

Unless otherwise stated, all solvents and chemicals were purchased from Bioshop Canada (Burlington, ON) and Sigma-Aldrich, and used without further purification. Desferoxamine mesylate salt was purchased from Santa Cruz Biotech, USA. The pH of the reaction solutions were tested using VWR pH paper.

High resolution mass spectra (HRMS) were obtained using Bruker MaXis 4G Q-ToF spectrometer. ^{1}H and 13C NMR were recorded on Bruker AV600 nuclear resonance spectrometers. ^{1}H and ^{13}C chemical shifts (δ) are reported in ppm relative to proton and carbon signals of the deuterated solvent, respectively. Coupling constants are reported in Hertz (Hz). Analytical high performance liquid chromatography (HPLC) was performed using Waters 2489 HPLC, Waters 2489 UV/Vis detector, and a model 106 Bioscan flow count gamma detector. Semi-preparative HPLC was performed using Agilent/Varian ProStar model 325 photodiode array (PDA) detector equipped with model 210 solvent delivery system. Analytical runs were performed using Synergi 4μ polar reverse-phase column (250 × 4.6 mm; 4 μm; Phenomenex; flow rate 1 mL/min; UV-Vis detection wavelength 280 nm). Semi-preparative runs were performed using Synergi 4μ polar reverse-phase column (250 × 10.0 mm; 4 μm; Phenomenex; flow rate 4 mL/min; UV-Vis detection wavelength 280 nm). HPLC eluent A consisted of 4% v/v acetonitrile in 2.5 mM triethylammonium acetate buffer (pH 6) while eluent B was 80% v/v acetonitrile in 2.5 mM triethylammonium acetate buffer (pH 6). Triethyammonium acetate buffers were prepared using 2.5 mM trimethylamine and 2.5 mM acetic acid. HPLC eluent C consisted of 0.01 M NH_4OAc in H_2O. HPLC eluent D consisted of neat acetonitrile. The HPLC elution gradients were as follows: *Method A*: gradient elution (0-1 min) 0% B, (1-15 min) 0-100% B, (15-16 min) 100% B, (16-19 min) 100-0% B, (19-25 min) 0% B. *Method B*: gradient elution (0-2 min) 20% B, (2-7 min) 20-50% B, (7-10 min) 50% B, (10-15 min) 50-85% B, (15-17 min) 85%, (17-20 min) 85-20% B, (20-25 min) 20% B. *Method C*: gradient elution (0-1 min) 0% B, (1-21 min) 0-70% B, (21-22 min) 70% B, (22-25 min)

70-0% B, (25-30 min) 0% B. *Method D*: gradient elution (0-5 min) 5% D, (5-20 min) 5-60% D, (20-22 min) 60% D, (22-23 min) 60-5% D, (23-30 min) 5% D.

3.2.1 Synthesis

Preparation of Sodium Acetate Buffer

Sodium acetate buffer was prepared by the addition of acetic acid to an aqueous solution of 1 M sodium acetate to reduce the pH to 5. $Ga(NO_3)_3$ (30mg/mL) was added to sodium acetate buffer.

Synthesis of 3,14,25-trihydroxy-2,10,13,21,24,32-hexaoxo-3,9,14,20,25,31-hexaazapentatriacontan-35-oic acid (2)

Desferoxamine mesylate salt **1** (0.5 g, 0.76 mmol) was added to a solution of succinic anhydride (1.7 g, 17 mol) in pyridine (7.5 mL) and the reaction stirred for 24 hours at room temperature. Pyridine was removed by rotary evaporation, NaOH (0.15 M, 100 mL, pH~12) added and the reaction allowed to stir at room temperature for 12 hours. Subsequently, HCl (12 M, pH~1) was added dropwise and the solution was cooled over ice whereupon a precipitate formed. The precipitate was collected by filtration and washed with dilute HCl (1 M, pH~1) to yield a white solid (463 mg, 92%).

Synthesis of N^1-(5-(4-((4-(1,2,4,5-tetrazin-3-yl)benzyl)amino)-4-oxobutanamido)pentyl)-N^1-hydroxy-N^4-(5-(N-hydroxy-4-((5-(N-hydroxyacetamido)pentyl)amino)-4-oxobutanamido)pentyl)succinamide (3)

Compound **2** (67.9 mg, 103 μmol) was added to a solution of PyBOP (70.6 mg, 136 μmol) in 3 mL DMSO and stirred at room temperature for 15 min. In a separate vial, diisopropylethylamine (21.5 μL, 123 μmol) was added to 3-(4-benzylamino)-1,2,4,5-tetrazine (9.2 mg, 41.0 μmol) solution in DMSO (3 mL) and the solution stirred for 15 min. Subsequently, the *N*-succinyl-DFO solution was added dropwise to the tetrazine solution and the mixture stirred overnight at room temperature.[22] The desired product was isolated using a C_{18} solid phase extraction (SPE) cartridge (Waters C_{18} Sep-Pak Plus, Waters Corp., Ireland) followed by semi-preparative HPLC (method B). t_R = 9.5 min. Yield 5.8 mg, 17%. Analytical HPLC (method B) t_R = 13.4 min. ^{1}H NMR (600 MHz, DMSO-d_6) δ=1.21-1.23 (m, 22H), 1.35-1.40 (m, 13H), 1.49 (m, 12H), 1.96 (s, 6H), 2.26 (t, 8H), 2.34-2.43 (m, 14H), 2.57 (t, 8H), 2.99-3.03 (m, 12H), 3.44-3.46 (m, 7H), 4.39 (d, 4H), 7.53 (d, 4H), 7.7-7.8 (m, 6H), 8.44 (d, 3H), 8.48 (t, 2H), 9.59 (s, 1H), 9.63 (1H, s), 1.058 (s, 1H). HRMS calc. for $C_{38}H_{57}N_{11}O_{10}$ $[M+H]^+$ 830.4525 found, 830.4522.

Synthesis of vancomycin-*trans*-cyclooctene (5)

Synthesis of vancomycin-TCO was adapted from a literature procedure.[16] TCO-NHS (5 mg, 18.7 μmol; Click Chemistry Tools, USA) was added to a solution of vancomycin hydrochloride hydrate **4** (63.9 mg, 43.0 μmol) and *N*,*N*-diisopropylethylamine (DIPEA) in DMSO (50 μL, 243 μmol). The solution was placed in

the dark and the reaction was stirred at room temperature overnight and the product isolated by semi-preparative HPLC (Method A) t_R = 8.2 min. HPLC fractions containing the product were combined and the solvent removed by rotary evaporation yielding a white solid (17 mg, 57%). HPLC (method B) t_R = 10.8 min. HRMS calc. for $C_{75}H_{87}Cl_2N_9$ $[M+H]^+$ 1600.5173; found, 1600.5233.

Synthesis of Ga-desferoxamine-*N*-succinyltetrazine (6)

$Ga(NO_3)_3$ (3.61 μmol, 30.8 μL) in NaOAc (pH 5, 1 M) buffer was added to a solution of desferoxamine-*N*-succinyltetrazine **3** in DMSO (1.20 μmol, 1 mg/mL) and the mixture stirred at 60 °C for 1 hour. The solution was stirred overnight cooling to room temperature. The crude mixture was diluted with 10 fold volume of water, loaded onto a C-18 Sep-Pak cartridge, and washed with water (10 mL). The desired product was eluted using acetonitrile and the solution evaporated to dryness by rotary evaporation and purging under N_2 gas. ^{1}H NMR (600 MHz, DMSO-d_6) δ 10.58 (s, 1H), 8.49 (br m, 1H), 8.45 (d, J = 8.4 Hz, 2H), 7.9-7.5 (br m, 2H), 7.61 (br m, 1H), 7.54 (d, J = 8.4 Hz, 2H), 4.39 (d, J = 6.0 Hz, 2H), 3.5-0.9 (br m, 42H), 1.96 (s, 3H). IR (KBr pellet) 3428, 2938, 1780, 1635, 1438 cm^{-1}; HRMS-ESI (*m/z*): $[M+H]^+$ calcd. for $C_{38}H_{57}N_{11}O_{10}Ga$: 896.3546, found 896.3573; t_R (Method B)= 13.4 min.

Synthesis of ^{67}Ga- Desferoxamine-*N*-succinyltetrazine (7)

1 mg/mL **3** (50 μL) in DMSO was added to a 250 μL solution of $^{67}GaCl_3$ (9.2 MBq; Nordion Inc., Vancouver, Canada) in 0.1 M HCl. The pH was adjusted to pH 5 by

adding sodium acetate buffer (1 M, 125 μL) after 15 minutes, followed by addition of 100 μL of PBS and the pH adjusted to 6-7 using NaOAc (1 M, 350 μL). Subsequently, H_2O (125 μL) was added to create a 1 mL solution. The formation of ^{67}GaDFOTz was confirmed by HPLC and co-injection of an authentic reference standard GaDFOTz. HPLC (method B) t_R = 13.4 minutes.

Synthesis of ^{67}Ga Desferoxamine-*N*-succinyltetrazine-*trans*-cyclooctenevancomycin (8)

Vancomycin-TCO in DMSO (35 μL, 7 mg/mL, 0.60 μmol) was added to a solution of ^{67}GaDFO-Tz (250 μL, 0.060 μmol, 0.05 mg/mL, pH 7) in PBS and 5% DMSO. Analytical HPLC was used to confirm the formation of the conjugate product. HPLC (method B) t_R = 11.0 minutes.

3.2.2 Log *D* Determination

Lipophilicity of the compounds were experimentally determined using 1-octantol:PBS (log $D_{7.4}$).[23]

3.2.3 *In vitro* uptake assays

A sample of *S. aureus* (ATCC #: 25923) in 20% glycerol preservation culture was added to 45 mL of iron-deficient Tris Minimal Succinate (TMS) medium and placed in an incubator overnight shaking at 300 rpm and 37 °C. The OD_{600} of the overnight culture was determined. A radioactive stock solution (1 stock solution:10 TMS dilution) in TMS was prepared. Radioactive media was prepared by adding **7** to 5 mL iron-deficient TMS

to generate a solution having a final concentration of 7.4 Bq/µL. For competitive blocking assay, non-radioactive Ga-DFO (50 µM) and **7** were added simultaneously to the TMS media.

For the uptake studies, samples were incubated at 37 °C with shaking at 300 rpm for 24 hours. Every hour (t=0 h to t=6 h) and at 24 h, 500 µL aliquot of media was removed and centrifuged (12 500 × G) for 1 min. Subsequently, 480 µL aliquot of the supernatant was removed while ensuring that the pellet was not disturbed and added to Ria plastic test tube (12 × 55 mm, PerkinElmer). The pellets were washed with 500 µL of ice-cold phosphate buffered saline (PBS, 1 ×, GE Healthcare Life Sciences) and centrifuged (12 500 × G) for 1 min. Similarly, 500 µL aliquot of the supernatant was removed and added to the same Ria plastic test tube. The pellet was lysed by re-suspension in 400 µL of 5% sodium dodecyl sulfate (SDS, *w/v*) for 45 minutes. 300 µL aliquot of lysed pellet was removed and collected in a separate Ria test tube. The activity counts per min (cpm) for the supernatants and pellets were obtained using a Wizard 1470 Automatic Gamma Counter (PerkinElmer) for 1 min. Uptake was expressed as the ratio of radioactivity in pellet over total activity present, as described in the following equation:

$$\%\ \text{uptake} = \frac{cpm(pellet)}{(cpm(pellet) + cpm(supernatant))} \times 100$$

The uptake was normalized to the protein concentration to account for cell growth during the experiments. The protein concentrations were determined in triplicates by Pierce™ BCA Protein Assay Kit. Bovine serum albumin was used as a standard.

3.2.4 Evaluation of *S. aureus* Binding for 8

For one-step labeling, compound **8** (37 kBq, 0.0074 kBq/μL) in PBS was added to *S. aureus* bacteria, and samples were incubated in TMS media at 37 °C with shaking at 300 rpm for up to 6 h. For blocking studies, unmodified vancomycin (250μL, 50μM) along with **8** was added to the cell culture. At 1 h and 6 h, samples were collected, and the activity in the supernatant and bacterial cells were determined.

3.2.5 Evaluation of *S. aureus* Binding for 5

For pretargeting, *S. aureus* bacteria was first incubated in TMS media containing **5** (5 mL, 20 μM) for 30 minutes at 37 °C with shaking at 300 rpm. Following the incubation, each culture was centrifuged (12 500 × G, 1 minute) and the supernatant was discarded, ensuring that the pellet was not disturbed. The pellet was re-suspended in 5 mL of TMS, centrifuged (12 500 × G, 1 minute), and the supernatant was similarly discarded. The pellet was re-suspended in 4.5 mL of **7** (37 kBq, 0.0074 kBq/μL). Samples were taken at 1 h and 6 h and counted using a Wizard 1470 Automatic Gamma Counter (PerkinElmer) for 1 min. The percent binding was determined using the following equation:

$$\% \text{ binding } = \frac{cpm(pellet)}{(cpm(pellet) + cpm(supernatant))} \times 100$$

3.2.6 *Staphylococcus aureus* bacterial inoculum

Overnight cultures of *S. aureus* (ATCC 25293, Cedarlane Laboratories Ltd., Burlington, ON) were grown in Luria Broth media (L7658, Sigma-Aldrich Canada, Oakville, ON) at 37 °C with shaking at 300 rpm. Bacterial cultures were centrifuged (10 000 × G) for 2 minutes. The supernatant was discarded and the pellets were washed with sterile Phosphate Buffered Saline (PBS; Invitrogen, Mississauga, ON) and centrifuged (10 000 × G) for 2 minutes. The supernatant was discarded and the pellets were re-suspended in sterile PBS to an appropriate concentration for mouse inoculation (2×10^8 colony-forming units (CFU)/mL).

3.2.7 Mouse model

Animal studies were performed in Biohazard Level 2 lab at McMaster University, Hamilton, Canada. Balb/c female mice (n=3, 6-7 weeks old) were purchased from Charles River Laboratories (Senneville, Qc, Canada). The animal experiments were approved by the Animal Research Ethics Board at McMaster University in accordance with Canadian Council on Animal Care (CCAC) guidelines. These experiments were performed by qualified personnel with strict compliance to the guidelines set by the Animal Research Ethics Board.

3.2.8 SPECT Imaging of 7 in a Mouse Infection Model Pretargeted with Vancomycin-TCO 5

Four female Balb/c mice (6 to 7 weeks old) were injected with *S. aureus* (50 µL; 1×10^8 CFU) into the right calf muscle. Vancomycin-TCO and ^{67}*Ga*DFO-Tz were formulated in saline containing 1% DMSO (205 µg/mL) and saline containing 1% DMSO and 10% ethanol, respectively. At approximately 23 hours post infection, all mice were administered with vancomycin-TCO via the tail vein (~1.1 mg/kg). Immediately after the vancomycin-TCO injection (~6 min), 100 µL of ^{67}*Ga*DFO-Tz (~38.6 MBq) was injected via tail vein into one mouse. The other 3 mice were administered ^{67}*Ga*DFO-Tz via the same method at approximately 1 (mouse 2), 3 (mouse 3) and 24 (mouse 4) hours post vancomycin-TCO injection (~39.9, 36.3 and 19.7 MBq, respectively). Prior to imaging at the McMaster Centre for Preclinical and Translational Imaging, mice were anaesthetized with 1% isoflurane and maintained under same conditions for the length of the SPECT and CT scans. Imaging was conducted on all mice at 1 and 24 hours post radioactive injection. On a Gamma Medica Ideas X-SPECT system (North Ridge, California), multiple SPECT acquisitions were completed for 32 frames over 360° at 10 seconds/frame for the 1 hour time point. For the 24 hour time point, the SPECT acquisitions for all mice except mouse 4 were completed for 32 frames 360° at 30 sec/frame. For the fourth mouse, the acquisitions were completed at 80 seconds/frame (32 frames). CT acquisitions consisted of 1024 projection angles acquired over 360˚ with 75 Kvp, 165 µA cone beam CT system. Cobra Exxim software (Feldkamp filtered backprojection cone beam reconstruction software) was used to

reconstruct the images at a voxel size of 155 microns and a matrix size of 512^3. A water-filled tube was included within each scan in order to convert the voxel values to Hounsfield units (HU). An OS-EM interactive reconstructed method (2 iterations/8 subsets) was used to reconstruct the SPECT data which was fused to the CT data using in house software. AMIDE software was used to analyze the images.

3.2.9 Bacteria Growth Assay

Following biodistribution and imaging studies, the spleen, left and right calf muscles from each animal were placed in a sterile specimen bag (VWR International, Mississauga, ON) with 1 mL of sterile 1× PBS and macerated using a heavy lead weight. The tissue slurry was serial diluted using sterile PBS and an aliquot was plated on LB agar plates (L7533, Sigma-Aldrich Canada, Co., Oakville, ON). Plates were incubated overnight at 37 °C and CFU counts were determined.

3.2.10 Biodistribution studies of 7

S. aureus inoculum was injected into the right calf muscle of Balb/c female mice (50 µL; 1×10^8 CFU/injection). At 20 hour post infection, **7 (**100 µL PBS, 1.30 MBq) was intravenously administered via tail vein. After 1 hour post injection, mice were anesthetized with 3% isoflurane and euthanized by cervical dislocation. Blood, kidneys with adrenals, liver with gall bladder, lymph nodes from leg, small intestine (with contents), spleen, left calf muscle (non-infected), right calf muscle (infected), and bladder and urine were collected, weighed and counted using a Wizard 1470 Automated Gamma Counter (PerkinElmer, Woodbridge, ON). Organ activity measurements were decay

corrected and normalized to time of dose preparation to determine injected dose per gram (i.e. %ID/g).

3.3 Results

DFO derivatives of succinic acid and tetrazine have been reported for labeling biomolecules including antibodies.[22] Here, we prepared a known DFO-tetrazine conjugate (Scheme 3.3) which offers the opportunity to use TCO modified vancomycin to promote localization of the radiometal at sites of bacterial infection. Briefly, DFO-succinic acid was prepared by adding DFO to succinic anhydride, where **1** was isolated in 92% yield. Subsequently, the commercially available tetrazine **2** was coupled to **1** using PyBOP. The product **3** was isolated by semi-preparative HPLC in 17% yield where characterization data matched literature values.[22]

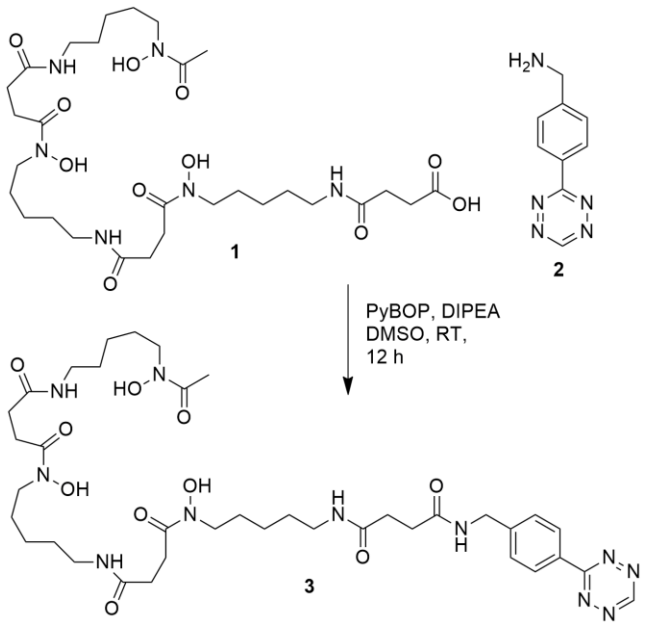

Scheme 3.3 Preparation of DFO-Tz **3**.

Briefly, vancomycin-TCO (Scheme 3.4) was prepared by adding vancomycin to a solution of TCO-NHS, where **5** was isolated by semi-preparative HPLC in 57% yield. The compound was characterized by HRMS and analytical HPLC and showed mass to charge (m/z) ratio and retention times in agreement with literature values. The compound was stored in the freezer and away from light as a solution in DMSO and remained stable over a period of 3 months.

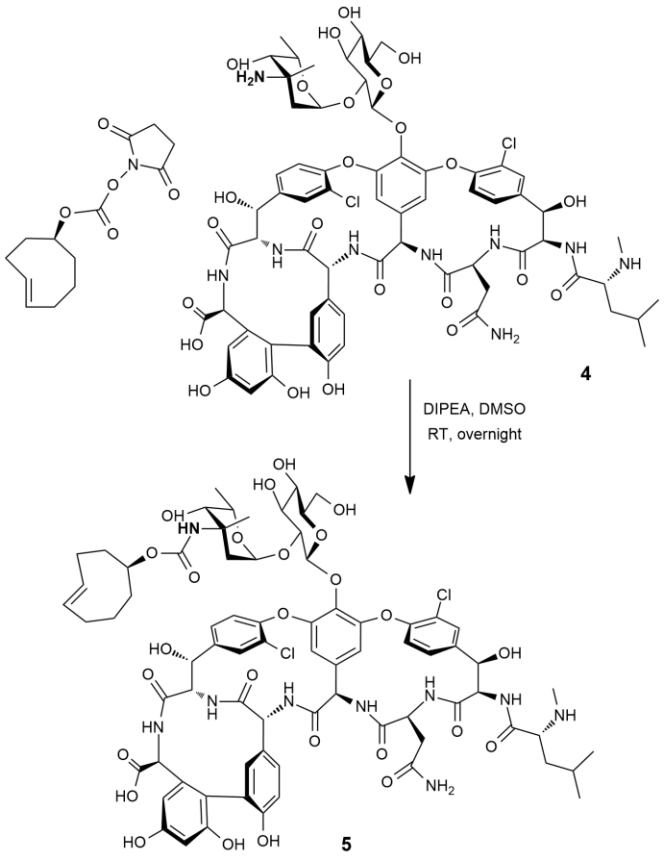

Scheme 3.4 Preparation of vancomycin-TCO **5**.

The cold Ga complex of **6** was prepared by combining **3** with $Ga(NO_3)_3$ and the product used as a reference standard for the radiolabeling studies (Scheme 3.5). Complexation of the DFO ligand was evident by ^1H NMR where N-OH signals were no longer present and the proton chemical shifts close to the hydroxamate functional group participating in chelation were significantly broadened. The HPLC chromatogram of **6** revealed a single peak and the HRMS data (m/z = 896.3586) corresponded with the expected value for **6**.

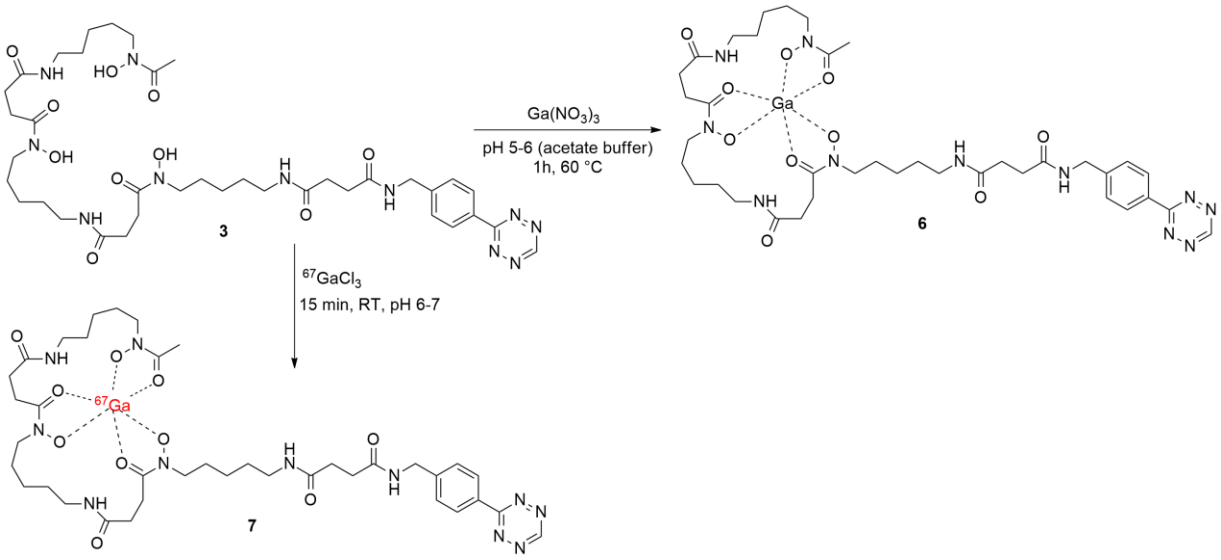

Scheme 3.5 Preparation of GaDFO-Tz **6** and ^{67}GaDFO-Tz **7** complexes.

The DFO-Tz **3** was labeled at room temperature using a method adapted from Petrik *et al.* Briefly, 50 µg of **3** was added to $^{67}GaCl_3$ (9.2 MBq) and the product was isolated by HPLC after 15 min at room temperature. The radiochemical yield was greater

than 90% and the radiochemical purity was greater than 95%, where a single peak was observed in the γ-HPLC chromatogram with its retention time matching the UV-HPLC chromatogram of the Ga reference standard (Figure 3.2).

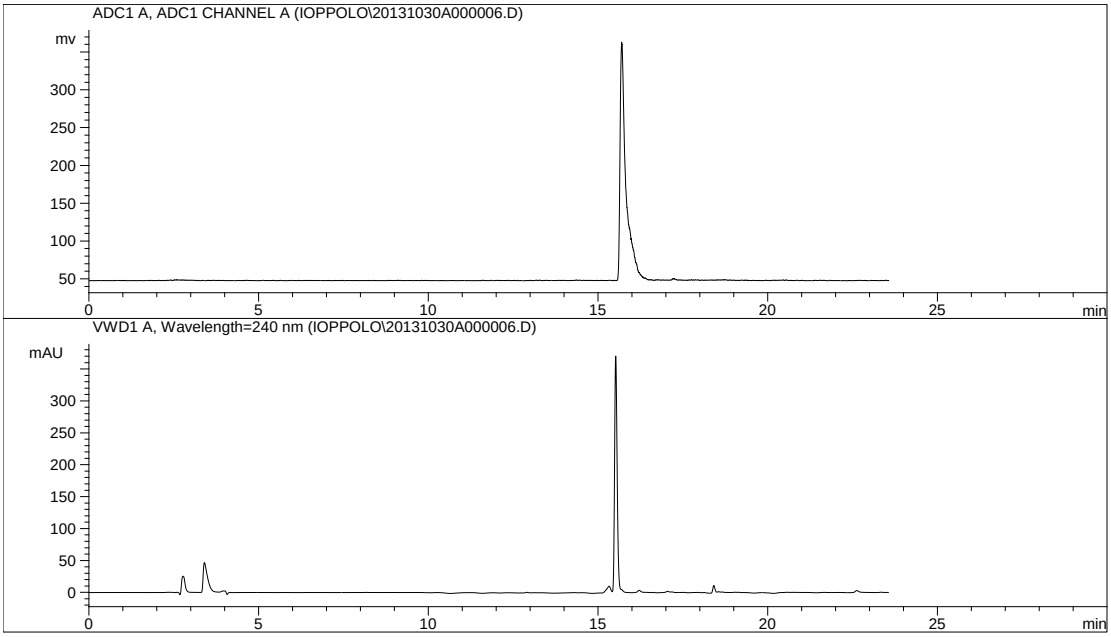

Figure 3.2 HPLC chromatograms (Method D) of **7** co-injected with **6**.

Radio-HPLC peak (top), UV chromatogram at λ = 240 nm (bottom).

3.3.1 Lipophilicity

Log $D_{7.4}$ of **7** and **8** were determined experimentally using 1-octantol:PBS following a literature procedure.[23] Log $D_{7.4}$ of **7** was calculated to be -0.78 ± 0.004 while

the log $D_{7.4}$ of **8** of was -1.86 ± 0.06. The log $D_{7.4}$ of the reference compound **1** was measured previously (Chapter 2) and was found to be -2.92 ± 0.04.

3.3.2 Stability Studies

The Stability of ^{67}GaDFO-Tz **7** and its ligation product **8** in 1× PBS at room temperature were studied using analytical HPLC. Minimal degradation of ^{67}GaDFO-Tz **7** was identified out to 24 h however, after one week at room temperature the purity decreased to 63%. In contrast, a formulation of the control compound **1** showed no detectable degradation after 7 days. This suggested that degradation of **7** was most likely due to the tetrazine which is known to have finite stability.[24] Stability of **8** was studied over 3 days where analytical HPLC revealed degradation as early as 7 hours (Figure 3.3). The purity dropped from > 99% to 62% by 7 hours and 45% by day 3.

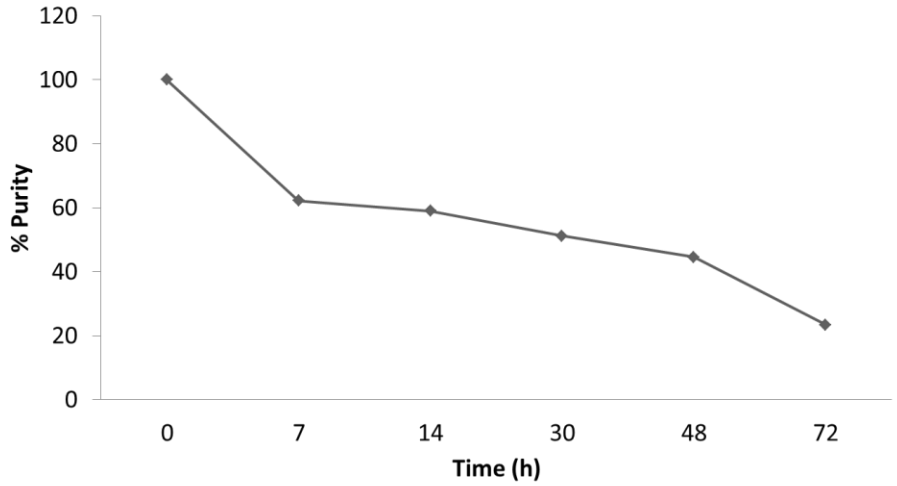

Figure 3.3 HPLC relative peak area of **8** over 3 days. HPLC (method B)

3.3.3 Detection of Bacteria *in vitro*

The ability of vancomycin-TCO to bind *S. aureus* was evaluated *in vitro* through both direct targeting and pretargeted approaches. The direct targeting approach involved combining vancomycin-TCO and ^{67}GaDFO-Tz before incubation with *S. aureus* at 37 °C for 6 h. The data showed 28% of the total activity was bound to *S. aureus* at 6 hours. *Escherichia coli* (*E. coli*) was used as a negative control where negligible binding (< 3%) was observed. For pretargeting which involved incubating *S. aureus* with vancomycin-TCO at 37 °C for 30 minutes before the addition of ^{67}GaDFO-Tz, the data showed 63% binding to *S. aureus*.

To prove the binding was due to specific interaction between the antibiotic and bacteria, GaDFO and unmodified vancomycin were added to the assays. The former is important to assess the extent of uptake of the tetrazine-metal complex in bacteria via the siderophore uptake pathway using ^{67}GaDFO-Tz alone (Figure 3.4). The experiments showed that ^{67}GaDFO-Tz had appreciable uptake (0.6% uptake/μg protein) relative to ^{67}GaDFO (0.9% uptake/μg protein). The uptake of ^{67}GaDFO-Tz was completely blocked by addition of GaDFO (1 mM) indicating that the small amount of uptake observed is through the siderophore uptake-related mechanism pathway.

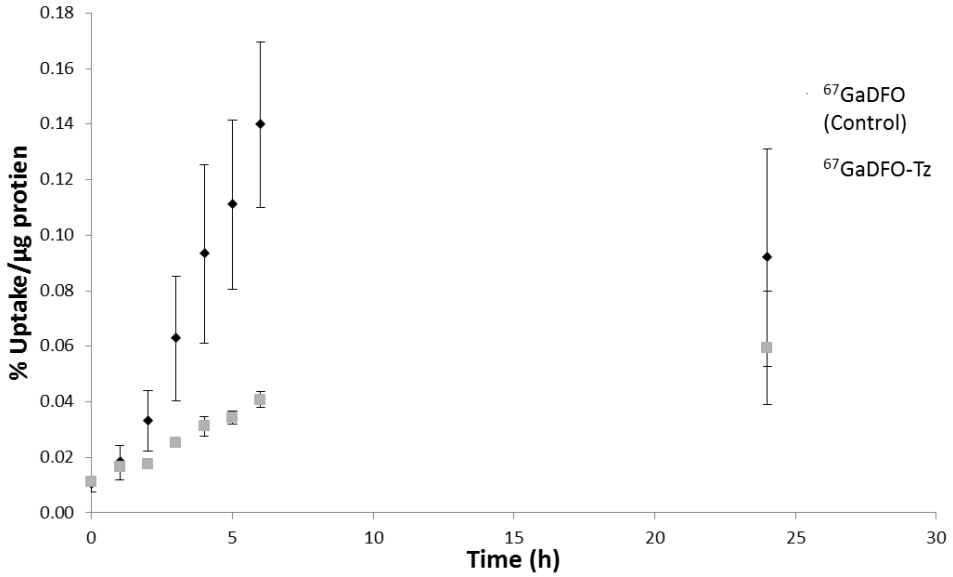

Figure 3.4 *In vitro* uptake of ^{67}GaDFO-Tz and GaDFO-Tz (block) by *S. aureus* over time. Note that all experiments were performed in duplicate.

Furthermore, blocking using GaDFO (1mM) would allow us to quantify binding based on the vancomycin-TCO and ^{67}GaDFO-Tz reaction. The results showed minimal (< 10%) impact with the addition of GaDFO. The addition of 200 µM unmodified vancomycin had a more pronounced impact on binding (Figure 3.5). Addition of unmodified vancomycin decreased binding from 63% to 1%.

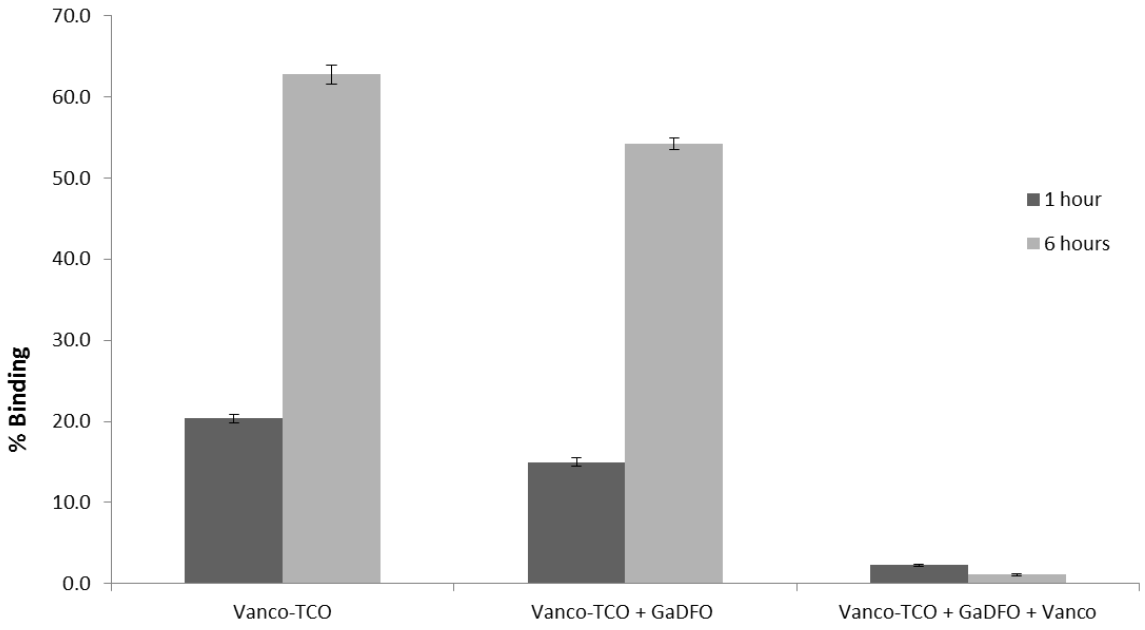

Figure 3.5 Plot of the percentage of ^{67}GaDFO-Tz **7** binding to *S. aureus* at 1 and 6 hours in the presence and absence of different blocking agents. Data shown are mean ± SEM (n=2).

3.3.4 SPECT/CT Imaging Studies

SPECT/CT imaging was used to evaluate direct targeting and pretargeting strategies in *S. aureus* infected murine models. Twenty-four hours following intramuscular administration of *S. aureus*, four mice were intravenously injected with vancomycin-TCO (~1.1 mg/kg). Mouse 1 was injected at 24 h post *S. aureus* infection after with ^{67}GaDFO-Tz, while mice 2 to 4 were injected between 24 and 27 hours post infection. SPECT/CT imaging was performed on all mice following 1 and 24 h post injection (p.i.) of ^{67}GaDFO-Tz. At 1 and 24 h imaging time points, all mice displayed

similar biodistribution results (see Supplementary data). The radioactivity was predominantly observed in the bladder for all mice at 1 h (Figure 3.6). At 24 h, the activity cleared from the bladder and largely resided in the liver. No activity was observed at the site of infection in mice 1 to 3. In contrast, radioactivity co-localized in the right calf muscle of mouse 4 at 24 h post injection of ^{67}GaDFO-Tz (Figure 3.6).

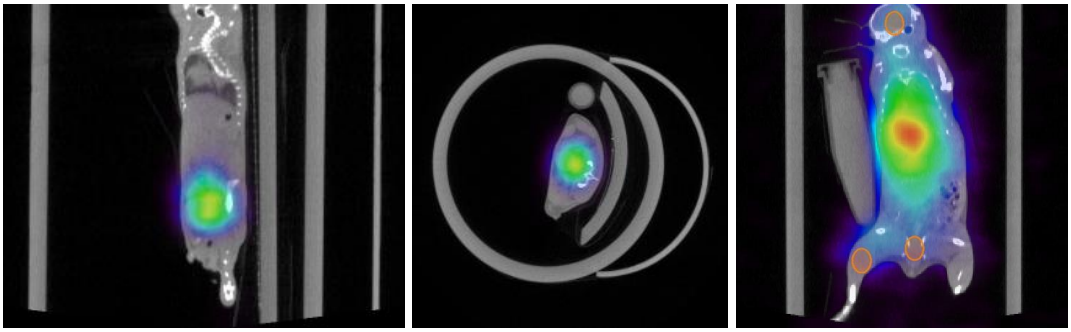

Figure 3.6 SPECT/CT sagittal (left), transverse (centre), and coronal (right) of mouse 4 after 1 h p.i. The red colour is the highest intensity. The orange circles are regions of interest.

3.3.5 Biodistribution Studies

Twenty-four hours following intramuscular administration of *S. aureus*, two cohorts of three mice were intravenously administered with ^{67}GaDFO-Tz or ^{67}GaDFO as a control. After 1 h, all mice were sacrificed and tissues collected. Biodistribution studies at revealed an infected calf muscle to non-infected calf muscle ratio of 6.3 for ^{67}GaDFO-Tz. Unfortunately, non-specific retention was observed in the small intestines with percent inject dose per gram (%ID/g) of 37.77 ± 5.73 and liver and gall bladder combined

of 2.93 ± 1.21 %ID/g (Table 3.1). The agent cleared through bladder which showed the highest uptake of 214.09 ± 100.96 %ID/g.

Table 3.1 Tissue distribution of 1 and 7 in *Staphylococcus aureus* mouse infection model at 1 h p.i. Data are expressed as ratios of %ID/g, expressed as the mean ± SEM (n=3).

Organs	**1**	**7**
Blood	0.07 ± 0.01	4.54 ± 4.42
Kidneys + Adrenals	1.75 ± 0.25	0.39 ± 0.02
Liver + Gall Bladder	0.11 ± 0.01	2.93 ± 1.21
Lymph Nodes	0.32 ± 0.16	0.05 ± 0.01
Small Intestine	0.63 ± 0.11	37.77 ± 5.73
Spleen	0.12 ± 0.01	0.81 ± 0.16
Calf Muscle (Left)	0.07 ± 0.01	0.04 ± 0.00
Calf Muscle (Right)	0.46 ± 0.12	0.20 ± 0.05
Urine + Bladder	381.75 ± 107.15	214.09 ± 100.96

For the pretargeting experiments, the bacterial counts were determined for spleen, infected calf muscle, and non-infected left calf muscle. The bacterial count for the infected calf muscle was measured to be 1.37×10^8 CFU by plating while negligible counts were measured in the non-infected calf muscle and spleen.

3.3 Discussion

Stability studies in 1× PBS at room temperature revealed minimal degradation of ^{67}GaDFO-Tz **7** by 24 hours. The degradation seen at later time points could be the result of tetrazine decomposition which is known to have finite stability. For example, Karver *et al.* have studied the stability of benzyl amino tetrazine in fetal bovine serum at 37 °C

over 10 hours and reported 60% degradation.[24] ^{67}GaDFO-Tz conjugate of vancomycin-TCO product **8** was also shown to have finite stability. Analytical HPLC traces revealed formation of new isomers with similar retention times 7 hours after preparation (see supplementary data). The conjugate product can rapidly rearrange and tautomerize to 1,4-dihydropyridazine in aqueous conditions as demonstrated in literature.[6,7] In presence of oxygen, the dihydropyridazine can oxidize to an aromatic pyridazine.[7] Therefore, the resulting peaks over time can be explained by the likeliness of conjugate product to isomerize or oxidize. However, this should not impact targeting or extent of binding.

The active uptake profile of ^{67}GaDFO-Tz was studied in *S. aureus* over 24 h. The rate of uptake of ^{67}GaDFO-Tz was slow for up to 6 h in comparison to control. At 24 h, the extent of uptake of both compounds (^{67}GaDFO-Tz and ^{67}GaDFO) is comparable. Furthermore, binding of vancomycin-TCO was studied via direct and pretargeted approaches. Pretargeting approach demonstrated superior labeling of *S. aureus* in comparison to the direct targeting approach. Therefore, the pretargeting approach is a successful candidate for *in vivo* labeling of *S. aureus*.

The binding of ^{67}GaDFO-Tz to *S. aureus* through direct targeting following ligation to vancomycin-TCO and pretargeted approaches was demonstrated. TCO modified vancomycin and the vancomycin-TCO conjugate employ the same binding mechanism as unmodified vancomycin which was demonstrated through blocking studies. The results showed that the bioorthogonal approach was more effective than direct targeting. More specifically, 63% binding was observed for pretargeting approach

while only 28% binding was observed for the direct targeting approach. The higher binding associated with the pretargeting approach may be associated with the extent of hydrogen bonding interactions of vancomycin to the acyl-D-alanyl-D-alanine amino acid component of Gram-positive bacterial cell walls[16] The larger size of the preformed conjugate may have reduced the extent of binding compared to vancomycin-TCO.

Evaluation of the pretargeting strategy *in vivo* binding of the bioorthogonal approach was performed in a murine model inoculated with *S. aureus*. At 71 h post infection, the radioactivity localized in the infected calf muscle of mouse; however, non-specific retention was observed in the liver and gall bladder. The main route of clearance of vancomycin in subjects with normal renal function is by glomerular filtration in the kidneys and renal excretion.[25] Imaging results were consistent and revealed the predominant route of clearance for the radioactivity in mice to be renal excretion. The *in vivo* studies revealed the pretargeting approach to be promising; however, identifying the optimal time for injection of radiolabeled tetrazine and the best dosage of vancomycin-TCO need to be determined.

As a control, the biodistribution of ^{67}GaDFO-Tz was also studied in a *S. aureus* murine model. ^{67}GaDFO-tetrazine showed comparable infected thigh to the non-infected to ^{67}Ga-DFO. Despite some accumulation of the imaging agent at the site of infection, non-specific binding was observed in the liver, gall bladder, and small intestines. Compound **7** showed comparable RT:LT ratios to ^{67}GaDFO. Future work will entail

evaluating the biodistribution of the pretargeting strategy to allow for direct comparison of the results (see chapter 4).

3.4 Conclusion

In summary, we have demonstrated the labeling of *S. aureus* can be achieved through a bioorthogonal approach between vancomycin-TCO and ^{67}GaDFO-Tz. However, further optimization is needed for the approach to be successful *in vivo*.

References

(1) Chen, K.; Chen, X. *Curr. Top. Med. Chem.* **2010**, *10*, 1227.

(2) Knight, J. C.; Cornelissen, B. *Am. J. Nucl. Med. Mol. Imaging* **2014**, *4*, 96.

(3) Chen, K.; Conti, P. S. *Adv. Drug Deliv. Rev.* **2010**, *62*, 1005–1022.

(4) Sletten, E. M.; Bertozzi, C. R. *Acc. Chem. Res.* **2011**, *44*, 666–676.

(5) Thalhammer, F.; Wallfahrer, U.; Sauer, J. *Tetrahedron Lett.* **1990**, *31*, 6851–6854.

(6) Blackman, M. L.; Royzen, M.; Fox, J. M. *J. Am. Chem. Soc.* **2008**, *130*, 13518–13519.

(7) Versteegen, R. M.; Rossin, R.; ten Hoeve, W.; Janssen, H. M.; Robillard, M. S. *Angew. Chem. Int. Ed. Engl.* **2013**, *52*, 14112–14116.

(8) Zeglis, B. M.; Sevak, K. K.; Reiner, T.; Mohindra, P.; Carlin, S. D.; Zanzonico, P.; Weissleder, R.; Lewis, J. S. *J. Nucl. Med.* **2013**, *54*, 1389–1396.

(9) Rossin, R.; Renart Verkerk, P.; van den Bosch, S. M.; Vulders, R.; Verel, I.; Lub, J.; Robillard, M. S. *Angew. Chemie Int. Ed.* **2010**, *49*, 3375–3378.

(10) Rossin, R.; Läppchen, T.; van den Bosch, S. M.; Laforest, R.; Robillard, M. S. *J. Nucl. Med.* **2013**, *54*, 1989–1995.

(11) Nichols, B.; Qin, Z.; Yang, J.; Vera, D. R.; Devaraj, N. K. *Chem. Commun.* **2014**, *50*, 5215–5217.

(12) Devaraj, N. K.; Thurber, G. M.; Keliher, E. J.; Marinelli, B.; Weissleder, R. *Proc. Natl. Acad. Sci.* **2012**, *109*, 4762–4767.

(13) Perkins, H. R.; Nieto, M. *Biochem. J* **1970**, *116*, 83–92.

(14) Nieto, M.; Perkins, H. R. *Biochem. J.* **1971**, *123*, 789–803.

(15) Van Oosten, M.; Schäfer, T.; Gazendam, J. a C.; Ohlsen, K.; Tsompanidou, E.; de Goffau, M. C.; Harmsen, H. J. M.; Crane, L. M. a; Lim, E.; Francis, K. P.; Cheung, L.; Olive, M.; Ntziachristos, V.; van Dijl, J. M.; van Dam, G. M. *Nat. Commun.* **2013**, *4*, 2584.

(16) Chung, H. J.; Reiner, T.; Budin, G.; Min, C.; Liong, M.; Issadore, D.; Lee, H.; Weissleder, R. *ACS Nano* **2011**, *5*, 8834–8841.

(17) Roohi, S.; Mushtaq, A.; Malik, S. A. *Radiochim. Acta* **2005**, *93*, 415–418.

(18) Wong, E.; Fauconnier, T.; Nguyen, T.; Pollak, A.; Rakhit, S. Glycopeptide-chelator conjugates, 2000.

(19) Matzke, G. R.; Zhanel, G. G.; Guay, D. R. P. *Clin. Pharmacokinet.* **1986**, *11*, 257–282.

(20) Brown, N.; Ho, D. H.; Fong, K. L.; Bogerd, L.; Maksymiuk, A.; Bolivar, R.; Fainstein, V.; Bodey, G. P. *Antimicrob. Agents Chemother.* **1983**, *23*, 603–609.

(21) Bunschoten, a; Welling, M. M.; Termaat, M. F.; Sathekge, M.; van Leeuwen, F. W. B. *Bioconjug. Chem.* **2013**, *24*, 1971–1989.

(22) Zeglis, B. M.; Mohindra, P.; Weissmann, G. I.; Divilov, V.; Hilderbrand, S. A.; Weissleder, R.; Lewis, J. S. *Bioconjug. Chem.* **2011**, *22*, 2048–2059.

(23) Wilson, A. A.; Jin, L.; Garcia, A.; DaSilva, J. N.; Houle, S. *Appl. Radiat. Isot.* **2001**, *54*, 203–208.

(24) Karver, M. R.; Weissleder, R.; Hilderbrand, S. A. *Bioconjug. Chem.* **2011**, *22*, 2263–2270.

(25) Moellering, R. C.; Krogstad, D. J.; Greenblatt, D. J. *Rev. Infect. Dis.* **1981**, *3*, S230–S235.

Chapter 4

4 Conclusions and Future Work

In summary, *in vitro* and *in vivo* studies revealed that ^{67}Ga complexes of simple DFO dertivatives were taken up by bacteria-specific siderophore pathway. Hence, this provides the opportunity to develop novel tracers for imaging infection based on ^{67}GaDFO using the bacteria-specific iron metabolism pathway. Despite their ability to bind *S. aureus in vitro*, biodistribution studies revealed that the current family of modified DFO derivatives are not optimal imaging agents due to their poor pharmacokinetic properties and clearance from non-target organs.

In an attempt to increase uptake, direct and pretargeting strategies were pursued both *in vitro* and *in vivo*. The work utilized the targeting properties of vancomycin derivative with ^{67}GaDFO through an inverse electron demand Diels-Alder cycloaddition reaction. The pretargeting approach revealed promising results, where 63% binding of ^{67}GaDFO-Tz to vancomycin-TCO bound to *S. aureus in vitro* was observed in comparison to 28% binding for the direct targeting approach.

Further optimization of the pretargeting time point for injection of ^{67}GaDFO-Tz and vancomycin-TCO concentration used are the next key steps. For the latter, the current dose was 1.1 mg of vancomycin-TCO/kg of mice. An additional goal is to

evaluate the pharmacokinetics of ^{67}GaDFOTz-TCOvancomycin *in vivo* to allow for direct comparison of direct and pretargeting strategies.

In addition to its use as an imaging agent, DFO has also been employed as a therapeutic adjuvant when chelated to gallium. *In vitro* experiments performed by Banin *et al.* examined biofilm formation in presence of sub-inhibitory levels of gentamycin, DFO, free gallium, and GaDFO on planktonic bacteria and biofilms.[1] Their results demonstrated the therapeutic properties of free gallium and GaDFO. This is due to the active uptake of GaDFO by bacteria which interferes with iron metabolism. Furthermore, free gallium can compete with iron for DFO resulting in similar interference with iron.[2] Unfortunately as aforementioned, DFO has poor pharmacokinetic properties and as a result, this approach cannot be translated to *in vivo*. It may be more effective to use one of the DFO derivatives or related analogue prepared using the new DFO functionalization chemistry reported here, which is another opportunity for future research.

Alternatively, following work published by Versteegen *et al.*, a novel drug releasing strategy was introduced that offers the opportunity to exploit both the therapeutic and imaging properties of GaDFO/^{67}GaDFO. In the work reported drug release was triggered by a bioorthogonal click reaction between TCO and Tz.[3] For the chemistry described here, the bioorthogonal reaction between Tz-TCO could be used to trigger the release of GaDFO/^{67}GaDFO at the site of infection.

To this end work to preparing a TCO-DFO conjugate **7** (Scheme 4.1) via carbamate linkage at the allylic position was explored. (*Z*)-Cyclooct-2-enol **3** was synthesized via a two-step reaction from the commercially available *cis*-cyclooctene **1**. 9-

Oxabiclo[6.1.0]nonane **2** was first synthesized through a reaction of *cis*-cyclooctene and sodium perborate tetrahydrate. The isolated product was subsequently treated with KOH at 95 °C for 47 h. The next step, which would be the focus of future work, involves isomerization of (*Z*)-cyclooct-2-enol **3** to (*E*)-cyclooct-2-enol **4** by irradiation with UV light for 32 hours. The isomer will be combined with 4-nitrophenylchloroformate to yield (*E*)-cyclooct-2-en-1-yl (4-nitrophenyl) carbonate **5**, which can subsequently react with DFO to yield the desired TCO-DFO product.[3]

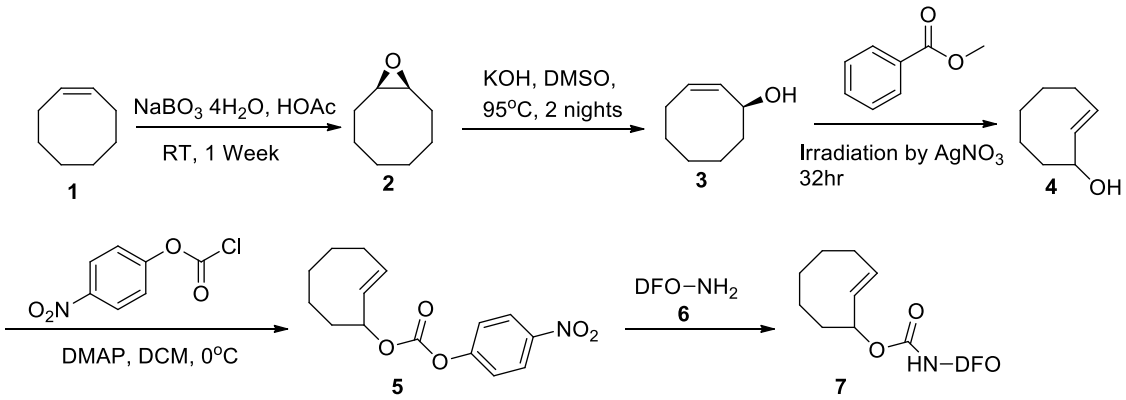

Scheme 4.1 Synthesis of **3** and proposed synthesis of TCO-DFO **7**.

The second component needed to explore a releasing strategy is the tetrazine-vancomycin conjugate **10**, which could be generated through a simple amide linkage (Scheme 4.2). Vancomycin-succinic acid precursor **8** was synthesized and isolated in 40% yield. So far, our attempts at conjugating vancomycin succinic acid **8** to tetrazine **9** using PyBOP as a coupling agent have been unsuccessful. This may be due to side reactions with other functional groups present on vancomycin. Identifying the optimal coupling conditions is the immediate next step prior to evaluation *in vitro* and *in vivo*

including comparison to the imaging strategies described in this thesis and gold standards such as radiolabeled leukocytes.

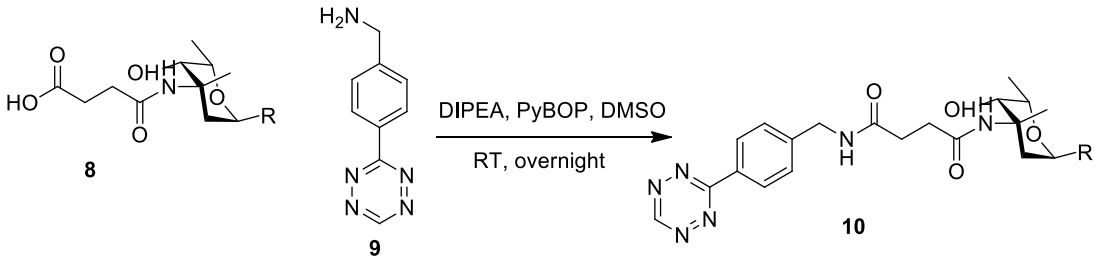

Scheme 4.2 Synthesis of **10** from the reaction between vancomycin-succinic acid precursor **8** and tetrazine **9**.

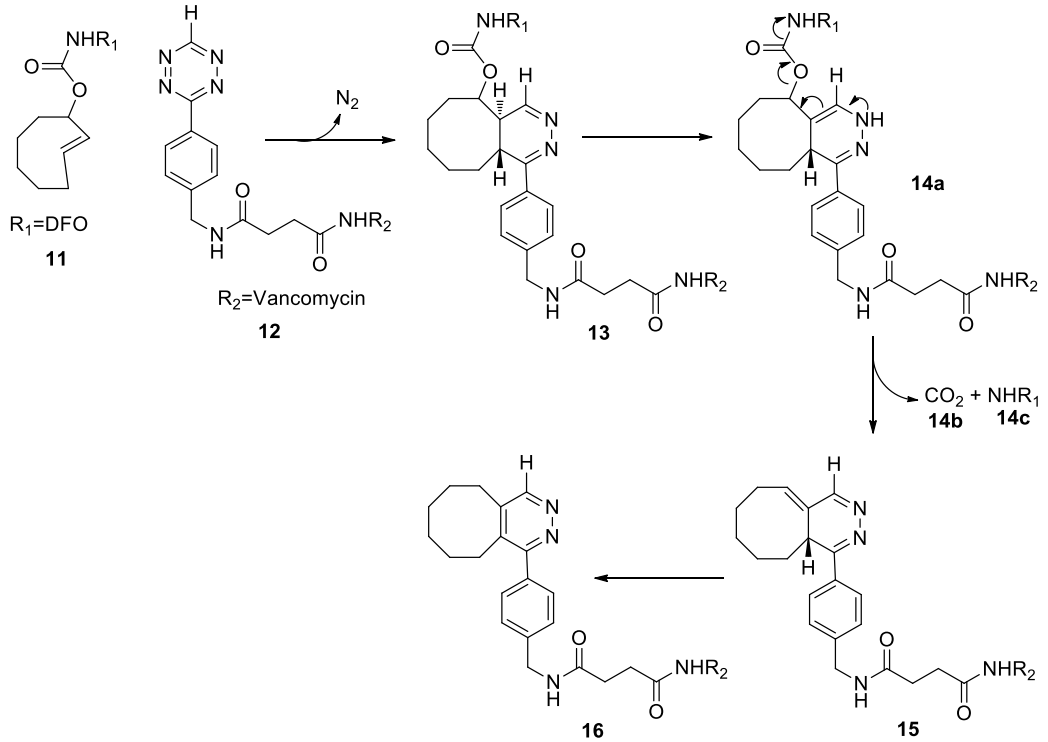

Scheme 4.3 Inverse-electron-demand Diels-Alder cycloaddition between **11** and **12**, and the potential mechanism for the release of GaDFO **14c**.

This system represents a potential route for using the Tz-TCO reactions to promote instantaneous release GaDFO/^{67}GaDFO at the site of infection. This may in turn enable GaDFO/^{67}GaDFO to concentrate at the site of the infection, thereby enhancing contrast and efficacy.

References

(1) Banin, E.; Lozinski, A.; Brady, K. M.; Berenshtein, E.; Butterfield, P. W.; Moshe, M.; Chevion, M.; Greenberg, E. P.; Banin, E. *Proc. Natl. Acad. Sci.* **2008**, *105*, 16761–16766.

(2) Zhai, C.; Summer, D.; Rangger, C.; Haas, H.; Haubner, R.; Decristoforo, C. *J. Label. Compd. Radiopharm.* **2015**, *58*, 209–214.

(3) Versteegen, R. M.; Rossin, R.; ten Hoeve, W.; Janssen, H. M.; Robillard, M. S. *Angew. Chem. Int. Ed. Engl.* **2013**, *52*, 14112–14116.